The GeV-TeV Galactic gamma-ray diffuse emission

I. Uncertainties in the predictions of the hadronic component

T. Delahaye[1], A. Fiasson[2], M. Pohl[3,4], and P. Salati[5]

[1] Instituto de Física Teórica UAM/CSIC Universidad Autónoma de Madrid Cantoblanco, 28049 Madrid, Spain
e-mail: `timur.delahaye@uam.es`
[2] LAPP, Université de Savoie, CNRS, BP110, F-74941 Annecy-le-Vieux Cedex, France
e-mail: `fiasson@lapp.in2p3.fr`
[3] Institut für Physik und Astronomie, Universität Potsdam, Karl-Liebknecht-Strasse 24/25, 14476 Potsdam, Germany
e-mail: `pohlmadq@gmail.com`
[4] DESY, Platanenallee 6, 15738 Zeuthen, Germany
[5] LAPTH, Université de Savoie, CNRS, BP110, F-74941 Annecy-le-Vieux Cedex, France
e-mail: `salati@lapp.in2p3.fr`

ABSTRACT

Context. The Galactic γ-ray diffuse emission is currently observed in the GeV-TeV energy range with unprecedented accuracy by the Fermi satellite. Understanding this component is crucial because it provides a background to many different signals, such as extragalactic sources or annihilating dark matter. It is timely to reinvestigate how it is calculated and to assess the various uncertainties that are likely to affect the accuracy of the predictions.
Aims. The Galactic γ-ray diffuse emission is mostly produced above a few GeV by the interactions of cosmic ray primaries impinging on the interstellar material. The theoretical error on that component is derived by exploring various potential sources of uncertainty. Particular attention is paid to cosmic ray propagation. Nuclear cross sections, the proton and helium fluxes at the Earth's position, the Galactic radial profile of supernova remnants, and the hydrogen distribution can also severely affect the signal.
Methods. The propagation of cosmic ray species throughout the Galaxy is described in the framework of a semi-analytic two-zone diffusion/convection model. The γ-ray flux is reliably and quickly determined. This allows conversion of the constraints set by the boron-to-carbon data into a theoretical uncertainty on the diffuse emission. New deconvolutions of the HI and CO sky maps are also used to get the hydrogen distribution within the Galaxy.
Results. The thickness of the cosmic ray diffusive halo is found to have a significant effect on the Galactic γ-ray diffuse emission, while the interplay between diffusion and convection has little influence on the signal. The uncertainties related to nuclear cross sections and to the primary cosmic ray fluxes at the Earth are significant. The radial distribution of supernova remnants along the Galactic plane turns out to be a key ingredient. As expected, the predictions are extremely sensitive to the spatial distribution of hydrogen within the Milky Way.
Conclusions. Most of the sources of uncertainty are likely to be reduced in the near future. The stress should be put (i) on better determination of the thickness of the cosmic ray diffusive halo and (ii) on refined observations of the radial profile of supernova remnants.

Key words. gamma rays: diffuse background – cosmic rays – methods: analytical – gamma rays: ISM

1. Introduction

The γ-ray sky at GeV-TeV energies is currently observed with unprecedented accuracy by the Fermi satellite (see for instance Knödlseder & for the Fermi/LAT Collaboration 2010). Among the various fields of investigation, the Galactic diffuse emission (Abdo et al. 2009) plays a very special role. Modeling that component is actually crucial for extracting a residual isotropic emission and may severely affect how the extragalactic γ-ray background is derived from observations. Theoretical errors in the predictions of the Galactic diffuse emission translate into systematic uncertainties on the extragalactic background and indirectly affect the studies of blazars and extragalactic active nuclei. The Galactic diffuse emission is also a natural background to many different signals, such as point sources or annihilating dark matter. Weakly interacting massive particles are actually one of the favored candidates for astronomical dark matter. They are expected to continuously annihilate within the Milky Way and to produce high-energy photons swamped inside the conventional Galactic diffuse emission. The latter needs to be accurately determined since it is the astrophysical background from which a possible dark matter contribution may have to be disentangled. The Galactic diffuse emission bears also upon searches for axion like particles or decaying gravitinos. It is thus timely to reinvestigate how it is calculated and to assess the various uncertainties that are likely to affect the accuracy with which it is derived.

The hadronic component of the Galactic γ-ray diffuse emission dominates the inverse Compton and the Bremsstrahlung mechanisms above a few hundred MeV (see for instance Stecker 1977; Strong et al. 2010; Strong 2011) supported by EGRET (Hunter et al. 1997) and Fermi (Abdo et al. 2009) observations. It is produced by the interactions of high-energy cosmic ray protons and

helium nuclei impinging on interstellar gas and is, as such, a probe of the distribution of hydrogen within the Galactic plane. It is also extremely sensitive to the distribution of cosmic ray primaries along the line of sight. Determining the hydrogen density from the Galactic diffuse emission requires thus knowing how protons and helium nuclei are distributed within the Galaxy. Cosmic ray transport is a key ingredient. In this article, it is described in the framework of a semi-analytic two-zone diffusion/convection model, which has been extensively discussed by Maurin et al. (2001); Maurin et al. (2002). This allows fast and reliable calculation of the γ-ray flux according to a procedure explained in section 2. Determining the hadronic component of the Galactic diffuse emission only requires a minute of CPU time on an ordinary PC. Notice that in Strong et al. (2010), although six different CR propagation models are considered and their effect on the γ-ray flux are investigated, no systematic analysis is presented.

A scan of the parameter space pertinent to cosmic ray transport and compatible with the boron-to-carbon data has been performed by Maurin et al. (2001), who find that many different propagation models are allowed by observations. In section 3, we take advantage of our semi-analytic derivation of the γ-ray flux to quantify the theoretical uncertainties arising from cosmic ray propagation. The effect of each parameter is scrutinized. The normalization and spectral index of the space diffusion coefficient are varied without much repercussion on the signal. Convection comes into play at low energies where it competes with diffusion. The overall effect on the γ-ray flux is moderate, though. More important are the dimensions of the cosmic ray diffusive halo whose radial and vertical extensions are varied. The larger the diffusive halo, the more abundant the hydrogen illuminated by cosmic ray protons and helium nuclei, and the stronger the diffuse emission. Variations in the γ-ray flux as large as 30% are found towards some directions when the half thickness L of the diffusive halo is increased from 1 to 4 kpc.

The uncertainties related to the nuclear cross sections and to the proton and helium fluxes measured at the Earth's position are investigated in sections 4.1 and 4.2. They are found to depend on the energy. In the former case, they amount to 33% at 1 GeV, reach a maximum of 54% at 4.5 GeV, and decrease down to 20 to 30 % above 100 GeV. In the latter case, they increase with energy to reach a value of ±37% at 1 TeV. We also derive the local effective γ-ray emissivity per hydrogen atom and compare our results to the recent Fermi measurements (Abdo et al. 2009). In section 4.3, we investigate how the distribution of primary cosmic ray sources along the Galactic plane affects the signal. We find that the radial profile of supernova remnants has a significant effect on the γ-ray diffuse emission, with variations as large as 50% towards the Galactic center and 70% in the opposite direction. We finally gauge the sensitivity of the Galactic γ-ray diffuse emission to the spatial distribution of hydrogen in section 5. The former is a probe of the latter and we find, as expected, that predictions depend significantly on the HI and CO three-dimensional (3D) maps selected for the calculation, as well as on the assumptions on the X_{CO} conversion factor. We base our predictions on new deconvolutions of the HI and CO sky maps (Pohl et al. 2008), which we compare to the hydrogen distributions provided by the GALPROP package (Strong & Moskalenko 1998). In section 6, we summarize the results of our analysis and outline the ingredients whose knowledge needs to be improved in order to make the Galactic diffuse emission an efficient probe of the distribution of hydrogen within the Milky Way.

2. Semi-analytic derivation of the gamma-ray flux

To derive the hadronic component of the Galactic γ-ray diffuse emission, we first express the flux at the Earth's position as a function of the γ-ray emissivities of the nuclei of the interstellar medium (ISM). The local effective emissivity $\mathcal{E}_{\rm eff}(\odot)$ of the ISM per hydrogen atom is computed and compared to the value observed recently by the Fermi collaboration (Abdo et al. 2009). The discussion of the uncertainties related to the γ-ray production cross sections and to the primary cosmic ray (CR) fluxes is postponed to sections 4.1 and 4.2. We then model the propagation of CR primaries within the magnetic fields of the Milky Way. This allows us to compute the proton and helium fluxes at any position $\mathbf{x}$ of the Galactic CR diffusive halo once these fluxes have been measured at the Earth's position. We finally explain how to speed up the calculation of the γ-ray flux by a careful selection of the integrals to be performed.

2.1. Gamma-ray emissivity of the interstellar medium

Above a few GeV, most of the γ-ray diffuse emission is produced by the interactions of CR protons and α particles impinging on the nuclei of the ISM. This yields the differential γ-ray flux at the Earth:

$$\Phi_\gamma(l, b, E) = \int_{\rm los} ds \left\{ n_{\rm H}(\mathbf{x}) \mathcal{E}_{\rm H}(\mathbf{x}, E) + n_{\rm He}(\mathbf{x}) \mathcal{E}_{\rm He}(\mathbf{x}, E) + n_{\rm C}(\mathbf{x}) \mathcal{E}_{\rm C}(\mathbf{x}, E) + \ldots \equiv \sum_{\rm A} n_{\rm A}(\mathbf{x}) \mathcal{E}_{\rm A}(\mathbf{x}, E) \right\}, \tag{1}$$

towards the direction defined by the Galactic longitude l and latitude b. The γ-ray energy is denoted by E. The flux Φ_γ involves the convolution along the line of sight (los) of the densities $n_{\rm A}$ of the various ISM elements with their γ-ray emissivities $\mathcal{E}_{\rm A}$. The position $\mathbf{x}$ is completely specified by b, l, and the depth s along the los.

When irradiated by high-energy CR species, the nuclei of the ISM shine in the γ-ray band. The rate at which a particular nucleus A produces high-energy photons of energy E per unit of energy and solid angle defines the emissivity $\mathcal{E}_{\rm A}$. This rate is expressed in units of photons $\rm s^{-1}\, sr^{-1}\, GeV^{-1}$. In the case of hydrogen for instance, the emissivity is given by the convolution of the impinging CR proton and helium fluxes Φ_p and Φ_α with the corresponding differential γ-ray production cross sections and may be expressed as

$$\mathcal{E}_{\rm H}(\mathbf{x}, E) = \int_{T_{min}}^{+\infty} dT \left\{ \frac{d\sigma}{dE}(p[T] + {\rm H} \to \gamma[E]) \times \Phi_p(\mathbf{x}, T) + \frac{d\sigma}{dE}(\alpha[T] + {\rm H} \to \gamma[E]) \times \Phi_\alpha(\mathbf{x}, T) \right\}. \tag{2}$$

The integral (2) runs over the kinetic energy *per nucleon* T of the projectiles.

The differential cross section $d\sigma/dE(p[T] + H \rightarrow \gamma[E])$ accounts for the interaction of a CR proton with kinetic energy T colliding upon a hydrogen nucleus of the ISM to yield a photon with energy E. At low T, typically below 2 to 3 GeV, one of the protons is excited into a Δ resonance, which subsequently decays back into a proton and a neutral pion (Stecker 1970), the latter yielding a pair of photons. The threshold for the production of the Δ resonance translates into the condition

$$T \geq \frac{\left(m_\Delta + 3m_p\right)\left(m_\Delta - m_p\right)}{2m_p} \geq T_{min} = 0.28 \text{ GeV}, \tag{3}$$

where the minimal value of the Δ resonance mass has been set equal to $m_\Delta = m_p + m_{\pi^0}$. At higher energies, deep inelastic scattering comes into play, and the isobaric approach needs to be gradually replaced with a scaling model accounting for quark interactions, hadronization, and pion production. The first parameterization of pion production in proton-proton collisions has been proposed by Stecker (1973) who compiled collider data, collected from 1956 to 1972, with beam energy up to ~ 1 TeV. The pion channel alone contributes 80% of the total photon yield. Other mesons, such as the charged and neutral kaons, come into play as do a few baryons, such as the Λ and Σ states, which are also produced in hadronic showers. Photons may also be directly generated in hadronic collisions. This process contributes even more than the other kaon and baryon channels over almost the entire energy domain and contributes 10 to 20% to the total photon yield. Based partially on the data collected by Stecker (1973), Kamae et al. (2006) propose a parameterization of the differential γ-ray production cross section in proton-proton collisions which is quite reliable below a projectile energy $E_p = m_p + T$ of order 50 GeV. Above that energy, the inclusive cross section for pion production, which Kamae et al. (2006) have borrowed from Blattnig et al. (2000), is significantly overestimated. Our article is based on the recent analysis by Huang et al. (2007). The Kamae et al. (2006) parameterization of the differential γ-ray production cross section in proton-proton collisions is used below a proton energy E_p of 2.5 GeV. Above $E_p = 20$ GeV, the photon production is given by the DPMJET-III Monte Carlo simulation of proton-proton, proton-nucleus and nucleus-nucleus collisions (Roesler et al. 2001; Roesler et al. 2001). The DPMJET-III event generator is a very reliable code at high energies. The requirement of unitarity, for instance, is built in, and no cross section becomes negative regardless of the energy. Although this code extrapolates low-energy data to higher energies, it has been used at CERN to calculate the shielding of the detectors and colliders. Between 2.5 and 20 GeV, Huang et al. (2007) interpolate linearly from the Kamae et al. (2006) parameterization and the DPMJET-III results. Because Huang et al. (2007) are interested in the production of γ-rays in an astrophysical environment, they have actually published the differential cross sections for CR protons or helium nuclei impinging on the ISM. In the former case, the cross section is defined as

$$\frac{d\sigma}{dE}(p + \text{ISM}) = \sum_A X_A \times \frac{d\sigma}{dE}(p + A) , \tag{4}$$

where the composition by number of the ISM has been set equal to $X_H = 0.9$, $X_{He} = 0.1$, $X_C = 2 \times 10^{-4}$, and $X_O = 4 \times 10^{-4}$. We assumed that composition to be constant throughout the Milky Way gaseous component.

The expression of the γ-ray flux at the Earth may be further simplified into a convolution along the los of the hydrogen density n_H with the effective emissivity $\mathcal{E}_{\text{eff}}$ of the ISM per hydrogen atom

$$\Phi_\gamma(l, b, E) = \int_{\text{los}} ds \, n_H(\mathbf{x}) \, \mathcal{E}_{\text{eff}}(\mathbf{x}, E) . \tag{5}$$

This effective emissivity, which encodes the ISM composition and the γ-ray production cross sections of the various nuclear channels, is related to the Huang et al. (2007) proton and helium cross sections through

$$\mathcal{E}_{\text{eff}}(\mathbf{x}, E) = \frac{1}{X_H} \int_{T_{min}}^{+\infty} dT \left\{ \frac{d\sigma}{dE}(p[T] + \text{ISM} \rightarrow \gamma[E]) \times \Phi_p(\mathbf{x}, T) + \frac{d\sigma}{dE}(\alpha[T] + \text{ISM} \rightarrow \gamma[E]) \times \Phi_\alpha(\mathbf{x}, T) \right\} . \tag{6}$$

The value of $\mathcal{E}_{\text{eff}}$ at the solar system is readily obtained by inserting the proton and helium fluxes observed at the Earth in the righthand side of expression (6). The red solid curve of Fig. 10 is based on the Shikaze et al. (2007) measurements and features $E^2 \mathcal{E}_{\text{eff}}$ as a function of photon energy E. The agreement with the Fermi data (Abdo et al. 2009) is fairly good, although the emissivity tends to be overpredicted. This is slightly puzzling since room must be left for other processes contributing to the γ-ray diffuse emission. Below 100 MeV, inverse Compton scattering and bremsstrahlung take over pion production. Although the former component has been substracted from the data, the hadronic emissivity cannot exceed the total emissivity, and the red solid line should be located below the Fermi points.

The detailed investigation of that apparent discrepancy will be presented elsewhere. Suffice it to say that the emissivity measured by Fermi is not strictly local but is an average over the regions of the Milky Way selected by Abdo et al. (2009) for their analysis. Those regions contain mostly atomic hydrogen and are located farther away from the Galactic center than the solar circle is. Although 85% of the gas along the los lies within 1 kpc from the Earth, the proton and helium fluxes to be used in relation (6) are smaller than the values borrowed from Shikaze et al. (2007). How much smaller is a crucial point on which depends the estimate of the bremsstrahlung contribution to the local γ-ray diffuse radiation field. Another possibility is to be found in the γ-ray production cross section itself. The Huang et al. (2007) parameterization could overestimate photon production below a few tens of GeV, a region where the Kamae et al. (2006) model provides a robust alternative. The uncertainty on the γ-ray emissivity induced by the existence of different choices for the γ-ray production cross section will be examined in section 4.1.

2.2. Cosmic ray transport throughout the Galaxy

The proton and helium fluxes are measured at the Earth but we need to know them at any point $\mathbf{x}$ along the los. Deriving $\Phi_p(\mathbf{x}, T)$ and $\Phi_\alpha(\mathbf{x}, T)$ from their solar circle values is mandatory and requires that we model the propagation of CR species inside the Galaxy. Regardless of the mechanism responsible for their production, charged particles propagate through the Galactic magnetic field and are deflected by its irregularities: the Alfvén waves. In the regime where the magnetic turbulence is strong – which is the case for the Milky Way – cosmic ray transport needs to be investigated numerically. Monte Carlo simulations (Casse et al. 2002) indicate that it is similar to space diffusion with a coefficient

$$K(T) = K_0 \, \beta \, (\mathcal{R}/1 \, \text{GV})^\delta \quad , \tag{7}$$

which increases as a power law with the rigidity $\mathcal{R} = p/q$ of the nucleus. In addition, because the scattering centers drift inside the Milky Way with a velocity $V_a \sim 20$ to 100 km s^{-1}, a second-order Fermi mechanism is responsible for some mild diffusive reacceleration. Its coefficient K_{EE} depends on the cosmic ray velocity β and total energy E and is related to the space diffusion coefficient $K(T)$ through

$$K_{EE} = \frac{2}{9} \, V_a^2 \, \frac{E^2 \beta^4}{K(T)} \quad . \tag{8}$$

Because K_{EE} is inversely proportional to K, the typical timescale for energy diffusion – which is given by the ratio E^2/K_{EE} – is much larger than the timescale associated to space diffusion for energies exceeding a few GeV per nucleon (GeV/n). As we are interested in the γ-ray diffuse emission in the GeV to TeV range, diffusive reacceleration can be safely disregarded since photons are produced by protons and helium nuclei with energies greater than 10 to 20 GeV/n. The proton and helium fluxes with which we derive the effective emissivity $\mathcal{E}_{\text{eff}}$ at the solar circle in sections 4.1 and 4.2 are simple power laws obtained by fitting the various CR data . These power laws do not exhibit any excess in the Gev region as we would have expected should diffusive reacceleration be efficient at sub-GeV scales. The γ-ray emissivity $\mathcal{E}_{\text{eff}}(\odot)$ that we obtain, is in fair agreement with the Abdo et al. (2009) measurements down actually to a photon energy of 100 MeV. Energy losses do not play any major role either since they replenish the low-energy regions of the CR proton and helium spectra where particles are already abundant. On the contrary, Galactic convection wipes cosmic rays away from the disk with a velocity $V_C \sim 5$ to 15 km s^{-1}. This process has some effect at low energy.

We assume that steady state holds for CR protons and helium nuclei. The master equation fulfilled by the space and energy distribution function $\psi = dn/dT$ of each of these CR species may be written as

$$\partial_z (V_C \, \psi) - K \, \Delta \psi = q(\mathbf{x}, T) \quad , \tag{9}$$

where energy losses and diffusive reacceleration have been neglected. This equation can be solved within the framework of the semi-analytic two-zone model, which has been extensively discussed in previous works such as Maurin et al. (2001) and Donato et al. (2001). According to this approach, the region of the Galaxy inside which cosmic rays diffuse – the so-called diffusive halo or DH – is pictured as a thick disk that matches the circular structure of the Milk Way. The Galactic disk of stars and gas, where primary cosmic rays are accelerated, lies in the middle. It extends radially 20 kpc from the center and has a half thickness h of 100 pc. Confinement layers where cosmic rays are trapped by diffusion lie above and beneath this thin disk of gas. The intergalactic medium starts at the vertical boundaries $z = \pm L$, as well as beyond a radius of $r = R_{\text{Gal}} \equiv 20$ kpc. The half thickness L of the DH is still unknown, and reasonable values range from 1 to 15 kpc. The diffusion coefficient K is the same everywhere, whereas the convective velocity is exclusively vertical with component $V_C(z) = V_C \, \text{sign}(z)$. This Galactic wind, which is produced by the bulk of the disk stars like the Sun, drifts away from its progenitors along the vertical directions. Also the normalization coefficient K_0, the index δ, the Galactic drift velocity V_C, and the Alfvén velocity V_a are all unknown. This situation can be remedied with the help of the boron-to-carbon ratio (B/C), which is quite sensitive to cosmic ray transport and which may be used as a constraint. The three propagation models featured in Table 1 have been drawn from Donato et al. (2004). The MED configuration provides the best fit to the B/C measurements, whereas the MIN and MAX models lead respectively to the minimal and maximal allowed antiproton fluxes, which can be produced by the annihilation of dark matter particles.

The axial symmetry of the DH leads naturally to expand the CR density ψ as a series of the Bessel functions $J_0(\alpha_i \, r/R_{\text{Gal}})$ where α_i is the i-th zero of the function J_0. This ensures that ψ vanishes at the radial boundary of the DH. The source term accounts effectively for both the production ($q > 0$) and the destruction ($q < 0$) of CR nuclei. The latter are accelerated by shock waves driven by supernova explosions taking place in the Galactic disk. The CR nuclei also undergo spallation reactions on the ISM, which depopulate the high-energy tails of their spectra. In the thin disk approximation, the source term may be expressed as

$$q(\mathbf{x}, T) = 2 \, h \, \delta_D(z) \, \{ \rho(r, z) \, Q_{\text{tot}}(T) - \Gamma \psi \} \quad , \tag{10}$$

where $\delta_D(z)$ is the Dirac function. We have assumed that the energy and spatial dependencies of the primary CR production rate can be disentangled. The space distribution $\rho(r, z)$ is discussed in section 4.3. It is normalized in such a way that $Q_{\text{tot}}(T)$ accounts for the total production of particles with kinetic energy per nucleon T over the whole Galaxy. In the case of protons, the spallation term is given by

$$\Gamma_p = v_p \, \{ \sigma_{p\text{H}} \, n_{\text{H}} + \sigma_{p\text{He}} \, n_{\text{He}} \} \quad , \tag{11}$$

where the densities n_{H} and n_{He} were averaged to 0.9 and 0.1 cm^{-3} respectively. The total proton-proton cross section $\sigma_{p\text{H}}$ has been parameterized according to Nakamura et al. (2010), while $\sigma_{p\text{He}}$ is related to $\sigma_{p\text{H}}$ by the Norbury & Townsend (2007) **scaling factor**

$4^{(2.2)/3}$. The velocity of protons with kinetic energy T is denoted by v_p. The master equation (9) simplifies considerably as long as z is different from 0. This leads to the solution

$$\psi(r, z, T) = \sum_{i=1}^{\infty} P_i(T) \times \exp\left(\frac{V_C |z|}{2K}\right) \times \left\{ \sinh\left[\frac{S_i}{2}(L - |z|)\right] / \sinh\left[\frac{S_i}{2}L\right] \right\} \times J_0(\alpha_i r/R_{\text{Gal}}) \quad, \tag{12}$$

where the inverse lengths S_i are defined by

$$S_i(T) = \sqrt{\left(\frac{2\alpha_i}{R_{\text{Gal}}}\right)^2 + \frac{V_C^2}{K^2}} \quad. \tag{13}$$

Bessel expanding the primary CR radial distribution $\rho(r, 0)$ and vertically integrating the complete master equation (9) through the thin disk allows, after some algebra, the Bessel transforms P_i to be expressed as

$$P_i(T) = \frac{q_i}{A_i} \times Q_{\text{tot}}(T) \quad. \tag{14}$$

The Bessel transforms q_i of the primary CR source radial distribution are related to $\rho(r, 0)$ through

$$q_i = \frac{1}{J_1^2(\alpha_i)} \times \frac{1}{\pi R_{\text{Gal}}^2} \times \left\{ \int_0^1 u \, du \, J_0(\alpha_i u) \, \rho(r = uR_{\text{Gal}}, 0) \right\} / \left\{ \int_0^1 u \, du \, \rho(r = uR_{\text{Gal}}, 0) \right\} \quad, \tag{15}$$

and do not depend on the CR energy. The coefficients A_i encapsulate the effects of space diffusion and Galactic convection as well as the spallations on the ISM. They are given by

$$A_i(T) = K S_i \coth\left(\frac{S_i L}{2}\right) + V_C + 2h\Gamma \quad. \tag{16}$$

The total CR production rates $Q_{\text{tot}}(T)$ are obtained by requiring that the proton and helium fluxes at the Earth, which in our model are defined as

$$\Phi_p(\odot, T) = \frac{1}{4\pi} v_p \psi_p(\odot, T) \quad \text{and} \quad \Phi_\alpha(\odot, T) = \frac{1}{4\pi} v_\alpha \psi_\alpha(\odot, T) \quad, \tag{17}$$

are actually equal to the fluxes Φ_p^{exp} and Φ_α^{exp} measured by the various CR experiments. In the case of protons, this translates into

$$Q_{\text{tot},p}(T) = \frac{4\pi}{v_p} \times \Phi_p^{\text{exp}}(T) \times \left\{ \sum_{i=1}^{\infty} \frac{q_i}{A_i} J_0(\alpha_i r_\odot/R_{\text{Gal}}) \right\}^{-1} \quad. \tag{18}$$

The galactocentric distance of the Earth $r_\odot$ has been set equal to 8.5 kpc. Our modeling allows us to *retropropagate* CR protons and helium nuclei from the Earth throughout the DH and to get $\Phi_p(\mathbf{x}, T)$ and $\Phi_\alpha(\mathbf{x}, T)$ everywhere along the los.

2.3. The basic relations for a fast calculation

Equipped with the above notations, we are ready to derive the hadronic component of the Galactic γ-ray diffuse emission. For a given photon energy E, each map requires five nested summations. We first need to scan through the Galactic longitude l and latitude b. Once a pixel is chosen, the effective emissivity $\mathcal{E}_{\text{eff}}$ of the ISM per hydrogen atom is integrated along the los. This emissivity results from the convolution in energy of the differential photon production cross sections with the proton and helium fluxes $\Phi_p(\mathbf{x}, T)$ and $\Phi_\alpha(\mathbf{x}, T)$. The latter are finally obtained from the expansion (12) over the corresponding Bessel coefficients $P_{p,i}(T)$ and $P_{\alpha,i}(T)$. If those five nested summations are performed by brute force, each map requires a few hours of CPU time on an ordinary PC. That is why we have taken advantage of the Bessel formalism to speed up the calculation. The idea is to never have more than three nested loops to compute at any time and to decompose the calculation in a few imbricated steps.

We first computed the Bessel transforms $P_{p,i}(T)$ and $P_{\alpha,i}(T)$ from our preferred parameterization of the proton Φ_p^{exp} and helium Φ_α^{exp} fluxes measured at the Earth's position – our reference model is based on Shikaze et al. (2007). The kinetic energy per nucleon T is varied from $T_{min} = 0.28$ GeV up to 10^3 TeV. We then point out that the radial and vertical dependencies factor out in the Bessel expansion (12). We may define the intermediate integral over the kinetic energy per nucleon as

$$\mathcal{I}_i(z, E) = \frac{1}{X_{\text{H}}} \int_{T_{min}}^{+\infty} dT \frac{v_{\text{nuc}}(T)}{4\pi} \times \tag{19}$$

$$\times \left\{ \frac{d\sigma}{dE}(p[T] + \text{ISM} \to \gamma[E]) \times P_{p,i}(T) \times \mathcal{V}_{p,i}(T, z) + \frac{d\sigma}{dE}(\alpha[T] + \text{ISM} \to \gamma[E]) \times P_{\alpha,i}(T) \times \mathcal{V}_{\alpha,i}(T, z) \right\} \quad,$$

which only depends on the Bessel order i and on the height z, once the γ-ray energy E has been selected. The function $\mathcal{V}_i$ captures the vertical behavior of the i-th term in the Bessel expansion (12) and is given by

$$\mathcal{V}_i(T, z) = \exp\left(\frac{V_C |z|}{2K}\right) \times \left\{ \sinh\left[\frac{S_i}{2}(L - |z|)\right] / \sinh\left[\frac{S_i}{2}L\right] \right\} \quad. \tag{20}$$
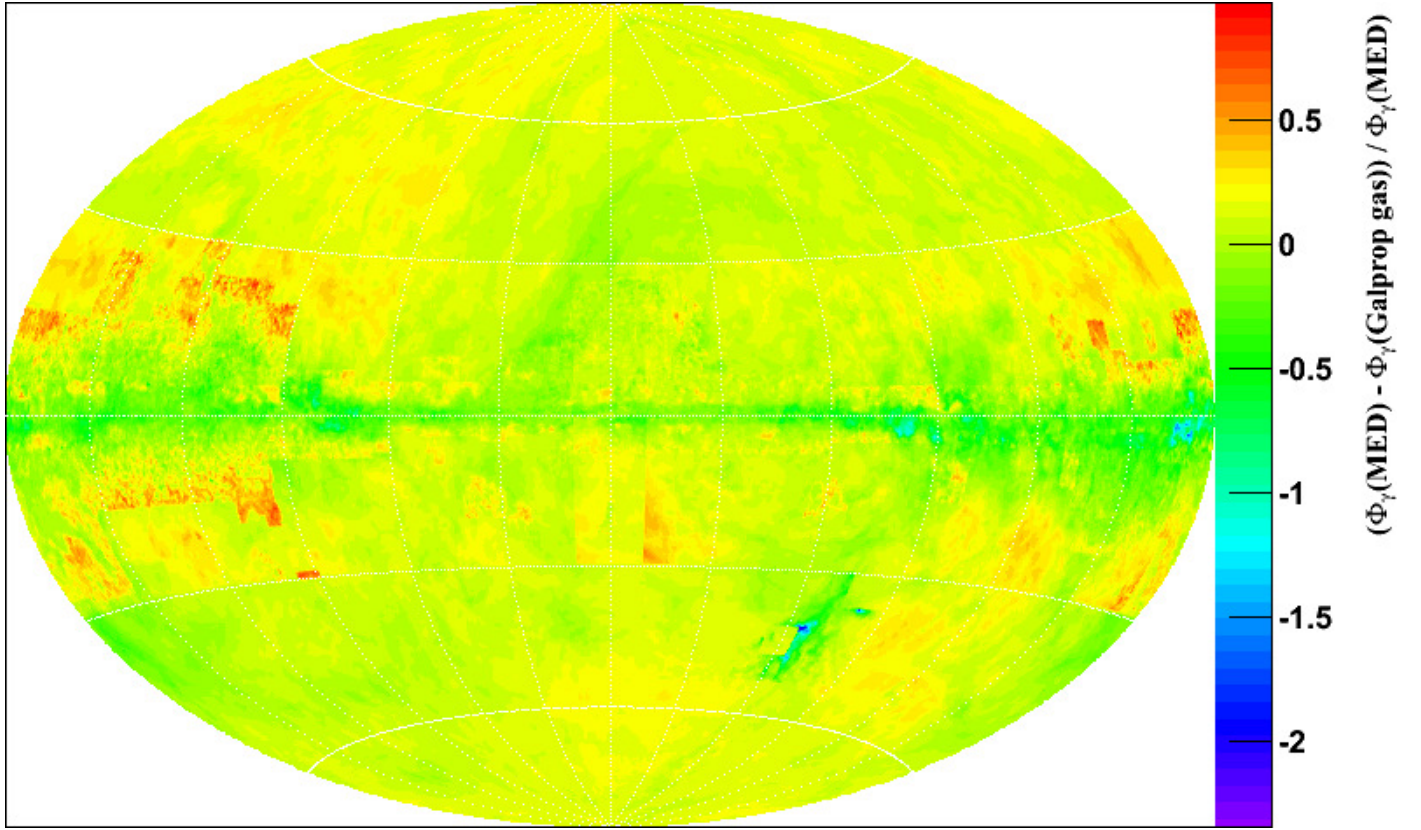
Fig. 1. Our reference map of the diffuse γ-ray emission of the Milky Way at 30 GeV obtained according to the method outlined in section 2. The dominant hadronic component alone is considered. The cosmic ray proton and helium fluxes at the Earth's osition are taken from Shikaze et al. (2007). These fluxes were *retropropagated* throughout the DH with the MED model of Table 1. The distribution of primary CR sources in the Galactic disk was borrowed from Lorimer (2004). The differential photon production cross sections of CR protons and helium nuclei impinging on the ISM were parameterized according to Huang et al. (2007). This map is based on the HI and CO 3D Galactic distribution of Pohl et al. (2008). The X_{CO} factor was set equal to 2.3×10^{20} molecules cm^{-2} (K.km.s^{-1})$^{-1}$ everywhere in the Galaxy.

We finally map the effective emissivity everywhere in the DH by computing the expansion

$$\mathcal{E}_{\text{eff}}(r, z, E) = \sum_{i=1}^{\infty} J_0(\alpha_i \, r/R_{\text{Gal}}) \times \mathcal{I}_i(z, E) \;, \tag{21}$$

up to a maximal Bessel order of 100. Relation (6) is recovered by combining equations (19) and (21). The γ-ray flux is then obtained by integrating along the los the hydrogen density n_H multiplied by the effective emissivity $\mathcal{E}_{\text{eff}}$, which we interpolate for any position $\mathbf{x}$ from its values on the r and z grid of expression (21). The entire process does not take more than a minute on an ordinary PC.

We followed this procedure to compute the reference map displayed in Fig. 1. The photon energy E was set equal to 30 GeV. The proton and helium fluxes at the Earth's position were parameterized according to Shikaze et al. (2007). These fluxes were *retropropagated* throughout the DH with the MED set of parameters of Table 1. The distribution of primary CR sources in the Galactic disk was borrowed from Lorimer (2004). The photon production differential cross sections of protons and helium nuclei impinging on the ISM were taken from Huang et al. (2007). We used the Galactic atomic and molecular hydrogen maps of Pohl et al. (2008). These maps were derived from the Kalberla et al. (2005) HI and composite Dame et al. (2001) CO surveys. The ionized hydrogen distribution were parameterized according to the Cordes & Lazio (2002) prescription. The X_{CO} factor was set equal to 2.3×10^{20} molecules cm^{-2} (K.km.s^{-1})$^{-1}$ everywhere in the Galaxy. The main thrust of this analysis was to vary individually each of the many parameters involved in the problem and to calculate the variations in the γ-ray flux relatively to our reference model.

3. Uncertainties arising from cosmic ray propagation

As explained in the previous section, the propagation of CR particles in the Galaxy is described by the four parameters K_0, δ, L, and V_C as long as diffusive reacceleration is not taken into account. The values of these parameters are not derived from first theoretical principles but are merely determined by a few ratios of secondary to primary CR abundances. The B/C has been used by Maurin et al. (2001) to considerably reduce the parameter space. Although more than 1,600 different sets of CR propagation parameters have been shown in Maurin et al. (2001) to be compatible with the B/C data, the three models featured in Table 1 provide a good indication of how uncertain Galactic CR propagation is. The extreme models MIN and MAX gauge the possible spread of values within which

the various parameters are to be found. As shown in Donato et al. (2004), these propagation models correspond respectively to minimal, medium, and maximal fluxes of primary antiprotons whose exotic dark matter species would produce everywhere inside the DH, if they exist. The more recent analysis by Putze et al. (2010) makes use of Monte Carlo techniques and gives similar results. That analysis confirms in particular that the half thickness L of the DH is not determined and may vary between 1 and 16 kpc. This also agrees, although to a somewhat lesser extent, with the conclusion reached by Trotta et al. (2011), who find that L may extend from 2 to 10 kpc. The uncertainties on CR propagation translate into uncertainties on the γ-ray flux. The spatial distributions of protons $\Phi_p(\mathbf{x}, T)$ and helium nuclei $\Phi_\alpha(\mathbf{x}, T)$ are modified if the propagation parameters are varied. If the DH itself is expanded and high values of L are selected, CR species may illuminate hydrogen far away from the Galactic disk, and the intensity of the γ-ray diffuse emission can be drastically increased.

Model	δ	K_0 [kpc²/Myr]	L [kpc]	V_C [km/s]	V_a [km/s]
MIN	0.85	0.0016	1	13.5	22.4
MED	0.70	0.0112	4	12	52.9
MAX	0.46	0.0765	15	5	117.6

Table 1. Typical combinations of CR propagation parameters that are compatible with the B/C analysis by Maurin et al. (2001).
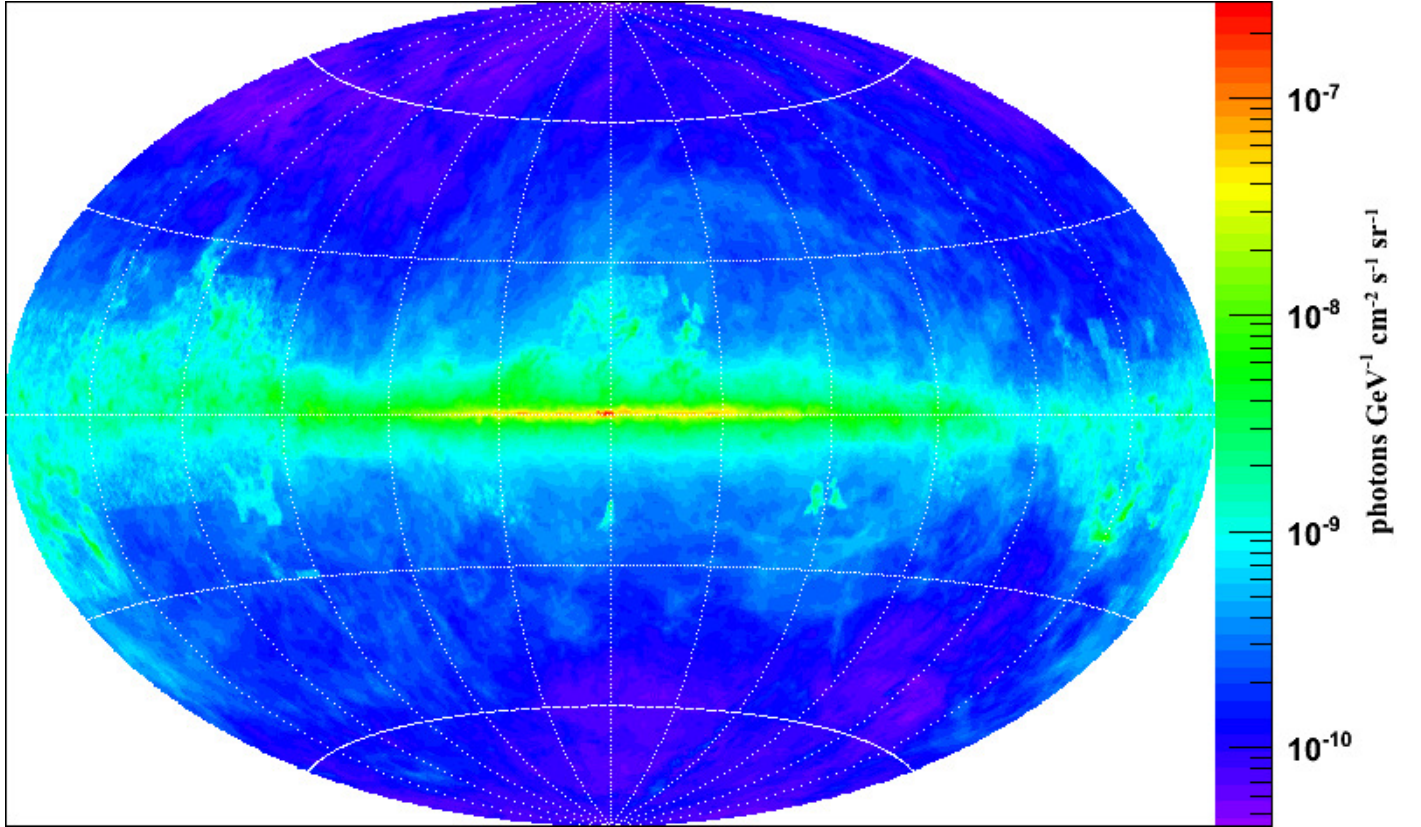

Fig. 2. This sky map features the difference between the MIN and MAX models relative to the MIN model. For each pixel we plotted the ratio (map1 − map2)/map1 where map1 (map2) has been derived exactly like the γ-ray reference map of Fig. 1 with the sole difference of using the MIN (MAX) propagation parameters instead of the MED model.

To get a sense of how important CR propagation is for the Galactic γ-ray diffuse emission, we plotted in Fig. 2 the difference between the MIN and MAX models relative to the MIN model. We first derived the γ-ray sky maps corresponding to the MIN and MAX sets of propagation parameters of Table 1 while keeping all the other inputs of the reference map of Fig. 1 unchanged – the latter is based on the MED model. We then computed the contrast

$$C = \left(\Phi_\gamma(\mathrm{MIN}) - \Phi_\gamma(\mathrm{MAX})\right)/\Phi_\gamma(\mathrm{MIN}) \; , \tag{22}$$

and plotted its value for each of the pixels of the map displayed in Fig. 2. As this map shows clearly, the uncertainty due to CR propagation can be quite important. For a photon energy of 30 GeV, the ratio of the MAX to MIN γ-ray fluxes varies over the sky from 0.63 to 2.26. The former value corresponds to a contrast C of +37% and to the red central region of the Galactic disk, while

the latter value is associated to a contrast of -126% and to a few dark blue spots located at fairly low Galactic latitude. We found that the contrast does not change much with energy in the GeV-TeV range. The map features four distinct colored regions.

(i) The contrast vanishes inside the yellow domains. These domains correspond to directions along which the gas is mostly nearby. The proton and helium fluxes are then approximately given by their values at the Earth. Whatever the CR model used to *retro-propagate* primary CR fluxes, we do not expect them to vary much in the neighborhood of the solar system, hence identical γ-ray emissivities and fluxes for the MIN and MAX configurations.

(ii) In the green regions, the contrast lies between -50% and -20% as indicated by the color scale on the righthand side of the map. The MAX γ-ray flux is 20% to 50% larger than the MIN one. This moderate difference can be interpreted if most of the gas that contributes to the signal is close to the Galactic plane. For the sake of the argument, we disregard all CR transport mechanisms except space diffusion and assume that the DH has no radial boundaries, which amounts to seting R_{gal} at infinity. We also concentrate on the 1D problem with CR densities depending only on the height z. The master equation (9) then yields the very simple solution

$$\frac{\Phi_p(\mathbf{x}, T)}{\Phi_p(\odot, T)} = \frac{\Phi_\alpha(\mathbf{x}, T)}{\Phi_\alpha(\odot, T)} = 1 - \frac{z}{L} \; , \tag{23}$$

where L is the half thickness of the DH. Values for that parameter range form $L_1 = 1$ kpc for the MIN model up to $L_2 = 15$ kpc in the MAX case. The γ-ray effective emissivity $\mathcal{E}_{\text{eff}}$ also scales as $1 - z/L$. If the fine-grained distribution of gas $n_H(\mathbf{x})$ that enters in relation (5) is now replaced by a homogeneous slab distribution extending from $z = -L_H$ to $z = +L_H$, the expression for the γ-ray flux boils down to

$$\Phi_\gamma \propto L_H - \frac{L_H^2}{2L} \; , \tag{24}$$

provided that $L_H \leq L_1$. The contrast is given by

$$- C = \frac{1 - (L_1/L_2)}{(2L_1/L_H) - 1} \; . \tag{25}$$

A contrast of -50% translates into a gas half thickness $L_H = 0.7$ kpc while a value of -20% implies $L_H = 0.35$ kpc. The green domains correspond to directions for which most of the gas is within 0.35 to 0.7 kpc from the Galactic plane.
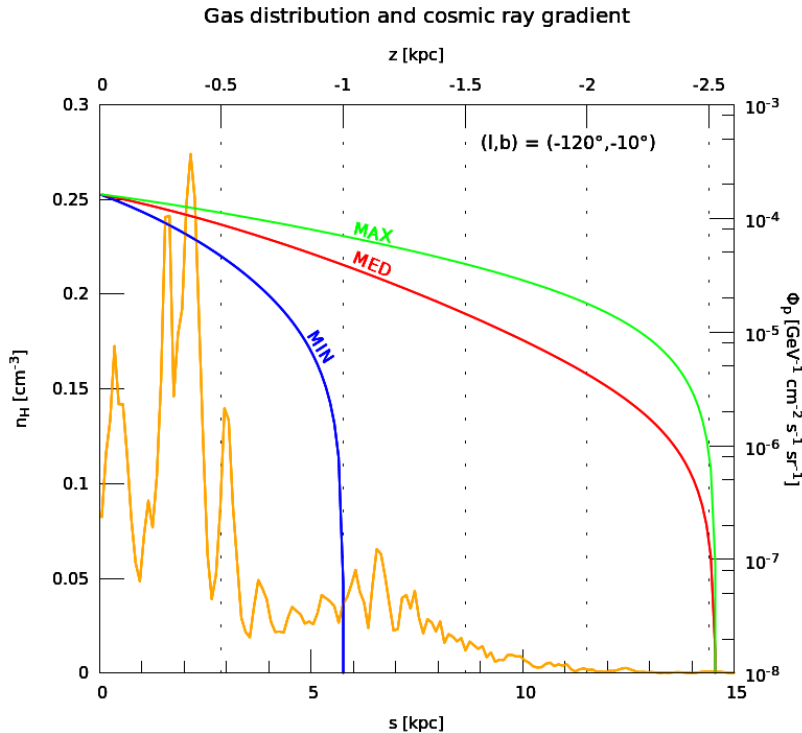

Fig. 3. The gas density (orange with units on the left y-axis) and the CR proton flux $\Phi_p(\mathbf{x})$ (units on the right y-axis) are plotted along the los in the direction specified by the Galactic longitude and latitude $(l, b) = (-120°, -10°)$. The three models of Table 1 have been considered for the calculation of the proton flux. They lead to the blue (MIN), red (MED) and green (MAX) curves. As an illustration, the CR proton total energy $E_p = m_p + T$ has been set equal to 30 GeV. The relative distribution of primary nuclei along the los is not expected to change much with energy.

(iii) Some regions of the sky seem more affected by CR propagation than others. The dark blue spots of Fig. 2 have a strong contrast with a MAX flux more than twice as large as the MIN one. Relation (25) indicates that L_H overcomes L_1 when the contrast is less

than -94%. Crudely speaking, the dark blue spots correspond to molecular clouds located farther away than 1 kpc from the Galactic plane. These clouds cannot be illuminated by CR protons and α particles in the MIN configuration because they are outside the DH. The density ψ of any CR species indeed becomes rapidly negligible near the boundary of the DH and vanishes completely outside. A careful inspection is necessary though. As is clearly illustrated in Fig. 3, the gas density, featured by the orange curve with units on the left vertical axis, is not at all negligible between $z = -0.7$ kpc and $z = -1.7$ kpc in the direction of the large spot beneath the Galactic plane at $(l, b) = (-120°, -10°)$. In the case of the MIN configuration, which corresponds to the blue line with units on the right vertical axis, CR protons cannot interact much with the gas located beyond a distance s on the los of 4 kpc. Behind that point, the gas clouds are too close to the vertical boundary of the DH to be strongly illuminated. For a distance s exceeding 6 kpc, the clouds are even outside the DH as their height z becomes less than $-L_1$. In the MED (red) and MAX (green) cases, the gas lying between $z = -0.7$ kpc and $z = -1.7$ kpc is, on the contrary, fully contained within the DH, hence a much larger γ-ray flux owing to a larger abundance of hydrogen producing it. We conclude that the blue spots correspond to clouds located typically beyond a distance to the Galactic plane of 0.7 kpc and lying therefore in a region where the MIN CR flux decreases rapidly, however, this effect is exaggerated by our sharp boundary conditions. In a model where the space diffusion coefficient K would vary with z like in Perelstein & Shakya (2010), the relative increase from the MIN to the MAX cases would not exceed a factor of 2.

(iv) Finally, the contrast C becomes positive in the central red region of the Galactic plane where $|l| \leq 60°$. In this part of the sky, the γ-ray flux derived from the MIN propagation set becomes larger than the flux obtained with the MAX model. This puzzling behavior is not surprising. The MIN set of parameters is associated to a strong convection and a weak space diffusion compared to the MAX case. The primary CR nuclei are blown away efficiently from the Galactic disk. They hardly make it to the Earth as they travel from the molecular ring, located at 4 kpc from the Galactic center, where most of the primary CR sources are found. In section 2.2, we have derived the proton and helium densities everywhere inside the DH by *retropropagating* these species back from the Earth where their fluxes are set equal to the values provided by observations. If convection in the MIN case prevents a substantial fraction of CR primaries to propagate from their sources to the Earth, the total Galactic production rates Q_{tot} need to be enhanced with respect to the MAX configuration in order to get the same proton and helium abundances at the solar circle. The sources need to be strengthened in the MIN case in order to give the observed proton and α fluxes at the Earth. The γ-rays are a unique probe of the CR densities inside the DH and not at the Earth only. Brighter CR sources in the MIN case translate into a more powerful illumination of the ISM in the direction of these sources. That is why the γ-ray diffuse emission from the inner parts of the Galactic disk is the brightest in the MIN model.
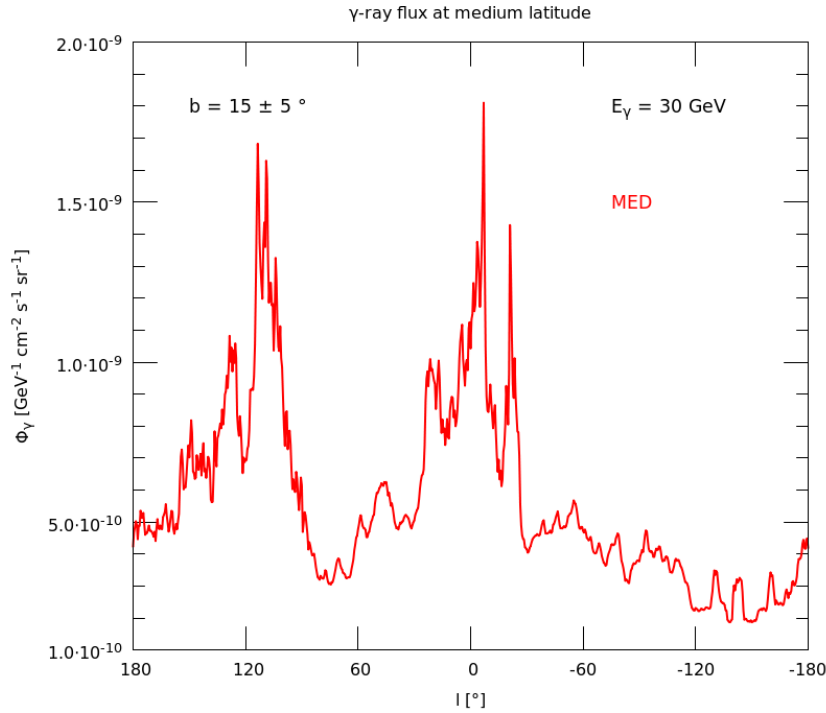

Fig. 4. The γ-ray flux of the reference map of Fig. 1 has been averaged over the Galactic latitude $10° \leq b \leq 20°$ and plotted as a function of Galactic longitude l. The photon energy is equal to 30 GeV. The Galactic CR propagation parameters correspond to the MED model of Table 1.

However, not all parameters have a priori the same impact on the γ-ray diffuse emission. That is why we systematically explored the effect of each of them. We first extracted the band $10° \leq b \leq 20°$ from the reference map of Fig. 1. That region has been studied in some detail by the Fermi collaboration (Abdo et al. 2009). We then averaged the γ-ray flux over Galactic latitude b and plotted the result in Fig. 4 as a function of Galactic longitude l. As in Fig. 1, the photon energy is 30 GeV. The flux varies up to a factor

of four from one longitude l to another. The gas distribution is far from homogeneous and the two peaks at $l = 0°$ and $l = 120°$ correspond to high concentrations of hydrogen along the los.
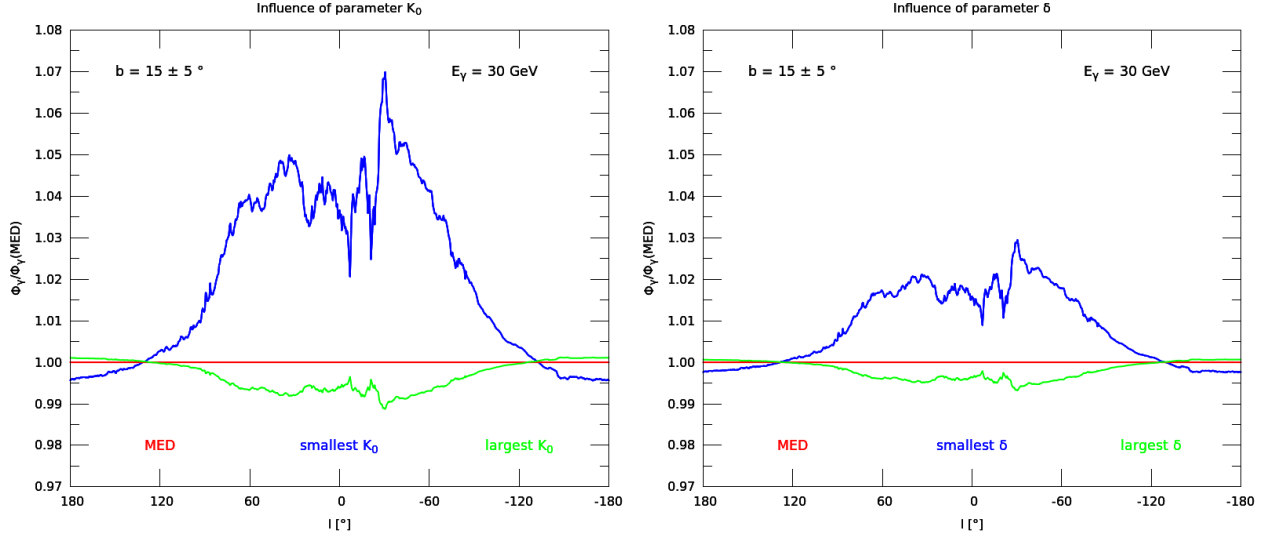

Fig. 5. Variations in the γ-ray flux relative to the reference case of Fig. 4. The red line is obtained when all the propagation parameters are extracted from the MED set of Table 1. *Left panel:* changing only the normalization K_0 of the space diffusion coefficient from its MED value to the lowest (1.6×10^{-3} kpc^2/Myr) and highest (7.65×10^{-2} kpc^2/Myr) values allowed by the B/C analysis yields the blue and green curves respectively. *Right panel:* same as in the left panel but varying the spectral index δ instead of the normalization K_0. The blue and green curves are derived from the smallest (0.46) and largest (0.85) values of the spectral index respectively.

As featured in the two panels of Fig. 5, varying the normalization K_0 or the spectral index δ of the space diffusion coefficient K has little impact on the γ-ray diffuse emission. At that latitude and for that energy, the variation reaches at most 7% and 3%. The strongest effect is obtained when either K_0 or δ is decreased. As space diffusion becomes less efficient, Galactic convection takes over, and the above-mentioned argument applies. More primary CR nuclei are washed out of the DH as they propagate from their production site, located at the molecular ring, to the Earth. The CR sources need to be slightly brighter than in the MED configuration in order to maintain the proton and helium fluxes at their terrestrial measured values, hence a larger γ-ray flux towards the Galactic center. For the same reason, the densities of CR protons and helium nuclei drop faster than in the MED case at large galactocentric distances, in the outer fringes of the DH. We anticipate a small drop in the γ-ray flux in the direction of the Galactic anti-center. This is exactly what the blue curves illustrate in each of the panels of Fig. 5. Those curves are above the reference red line for a Galactic longitude in the range $-120° \leq l \leq 120°$, while they exhibit a small deficit towards the Galactic anti-center. The green curves feature the opposite behavior. Space diffusion becomes more efficient than in the MED case, and the convection argument can be reversed with slightly fainter CR sources and a small deficit of the γ-ray flux at small Galactic longitudes.

If Galactic convection is now amplified with respect to the MED reference case while keeping all the other parameters fixed, we would expect the same effect as if space diffusion were inhibited. According to our reasoning based on the competition between convection and diffusion, an increase of V_C forces the Galactic primary CR production rates Q_{tot} to be higher in order to maintain the proton and helium fluxes at the Earth's position at their measured values. Convection prevents CR particles from propagating along the Galactic disk and wipes them out along the vertical directions of the DH. The molecular ring becomes brighter, and the γ-ray emission from that region is enhanced. The green curves of Fig. 6 correspond to a Galactic wind of 14 km/s and are located above the MED red lines. The increase is quite small insofar as V_C has just been slightly increased from its MED value of 12 km/s. If V_C is now decreased down to 5 km/s, we get the blue curves located below the reference red lines. The effect is more significant, although it does not exceed 0.5% at 30 GeV (left panel). At lower γ-ray energies, the CR proton and α particles implied in the photon production also have lower energies and diffuse less efficiently throughout the Milky Way magnetic field. Convection becomes relatively more important with respect to diffusion. The same variations of V_C are then expected to have a stronger impact on the γ-ray flux. This is exactly what the right panel of Fig. 6 illustrates. The photon energy has been set equal to 1 GeV. The blue line indicates a maximal variation of 5% at $l = -30°$, one order of magnitude more than in the left panel where $E = 30$ GeV. Finally the various curves of Figs. 5 and 6 all have the same shape. In particular, the blue and green lines are symmetrically drawn around the red axes.

Convection has an even greater impact at 100 MeV as shown in the left panel of Fig. 7 where the Galactic latitude b has been set equal to $0° \pm 5°$. This plot displays the variations in the γ-ray diffuse emission along the Galactic plane as the wind velocity V_C is increased up to 14 km/s or decreased down to 5 km/s. In the former case and for reasons already discussed above, the molecular ring becomes clearly visible. The green curve actually overcomes the red axis for a longitude $5° \leq |l| \leq 85°$, and the deficit in the direction of the Galactic center at $-5° \leq l \leq 5°$. The CR proton and helium nuclei located inside the molecular ring, at galactocentric distances less than ~ 4 kpc, are not as abundant as in the MED reference situation. The enhanced convection blows them away as
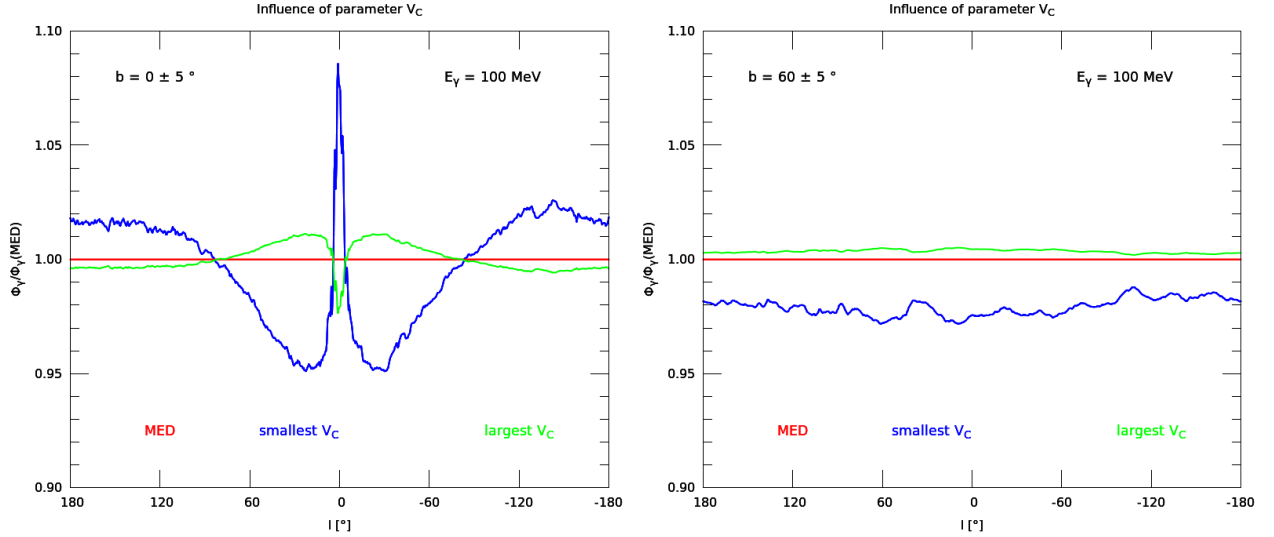
Fig. 6. Same as in Fig. 5 but varying the convective wind velocity V_C instead of the normalization K_0 or the spectral index δ of the space diffusion coefficient. The blue and green curves correspond to the lowest (5 km/s) and highest (14 km/s) values of V_C respectively. While fairly small at 30 GeV (left panel), the effect increases at 1 GeV (right panel).
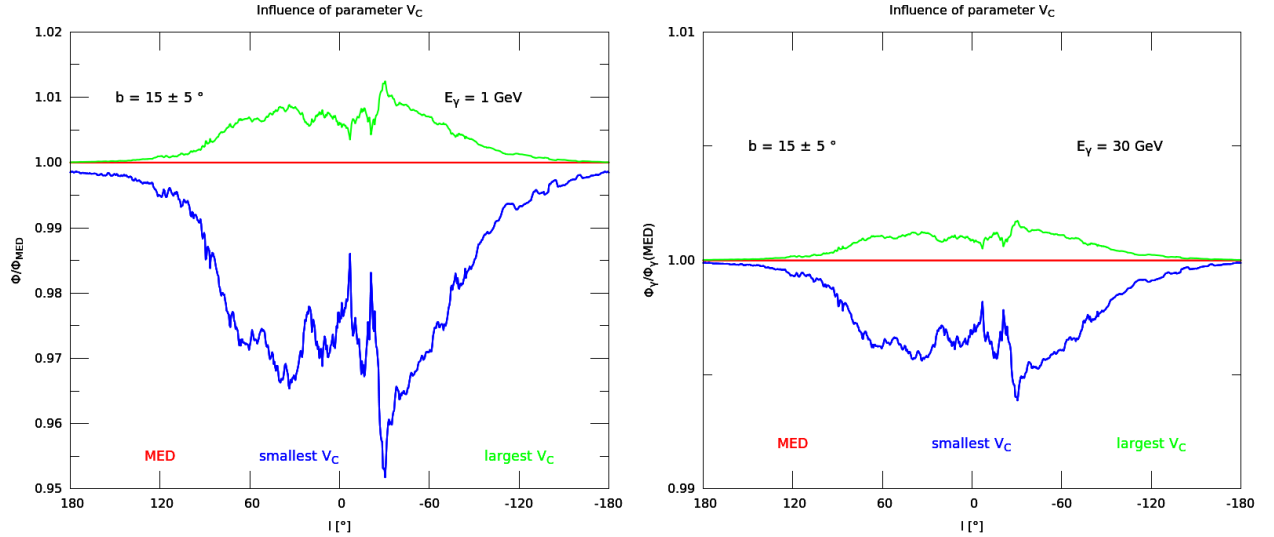

Fig. 7. Same as in Fig. 6 but for a γ-ray energy of 100 MeV and at latitudes of $0°$ (left panel) and $60°$ (right panel). The effect of convection is greatest along the Galactic plane and fades as the height $|z|$ increases.

they diffuse inwards from the molecular ring so that the Galactic center is underpopulated compared to the MED case. The blue line features the opposite behavior with a marked peak at the Galactic center where CR primaries are now more abundant. The overall effect does not exceed 9%, however. The Galactic plane is more sensitive to convection than high latitude regions where diffusion tends to homogenize cosmic rays. In the right panel of Fig. 7, the latitude has been set equal to $60° \pm 5°$. The green (blue) curve is still above (below) the red reference axis as a signature of the higher (lower) primary proton and helium nuclei production rates Q_{tot}. The variations in the γ-ray flux do not exceed 3%. We finally decreased the photon energy down to 10 MeV, well below the energy range to which this analysis is devoted. At these very low energies, the whole sky becomes equally sensitive to the value of V_C but the effect remains less than 10%.

We have so far varied the magnitude of Galactic CR convection or diffusion. We have studied the interplay between these two propagation mechanisms and showed that their impact on the γ-ray diffuse emission is small to moderate. We now explore how a change in the size of the DH itself would affect the γ-ray flux. In Fig. 8, the variations in the latter are averaged over the same interval of Galactic latitude as in Fig. 4. When L is decreased from its MED value of 4 kpc down to 1 kpc, the thickness of the DH has considerably shrunk. Hydrogen clouds lying at a height $|z|$ greater than 1 kpc are no longer illuminated by CR proton and helium nuclei. The amount of gas that participates in the signal is smaller in the MIN case than in the MED configuration although most of the Galactic hydrogen lies within the plane of the Milky Way. As shown by the blue curve, the reduction in the γ-ray emission may reach 30% in directions where a substantial fraction of the gas lies outside the DH. We have already witnessed that effect in the form of the dark blue spots in Fig. 2. In the MIN case, the CR proton and helium nuclei just miss the clouds located beyond the vertical boundaries of the DH as illustrated in Fig. 3. When L is increased to its MAX value of 15 kpc, the γ-ray emission becomes stronger,
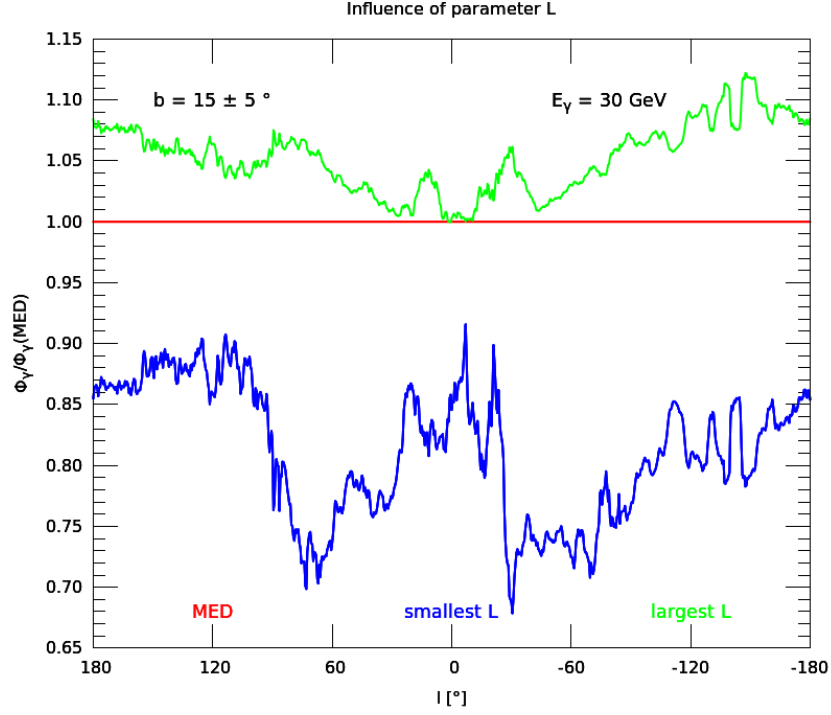
Fig. 8. The half thickness L of the DH was varied with respect to the MED configuration while keeping all the other parameters fixed. The green and blue curves correspond to the largest (15 kpc) and smallest (1 kpc) values of L, respectively. The red axis stands for the reference case (4 kpc). The variations in the γ-ray diffuse emission are drastic.

as expected. However, because most of the Galactic hydrogen lies within a distance $L_H \leq 0.7$ kpc from the disk, the enhancement of the γ-ray flux is moderate and does not exceed 8% in the direction of the Galactic center and 12% towards the anti-center. The DH acts as a reservoir for Galactic hydrogen. The larger its volume, the more gas that is illuminated by primary CR nuclei and the larger the signal. The latter has the same variations with L as the antiproton or positron yields of the putative particles that are supposed to make up the astronomical dark matter and to annihilate within the Milky Way. That is why we have featured in Table 1 the typical sets of propagation parameters borrowed from the dark matter primary antiproton analysis of Donato et al. (2004).
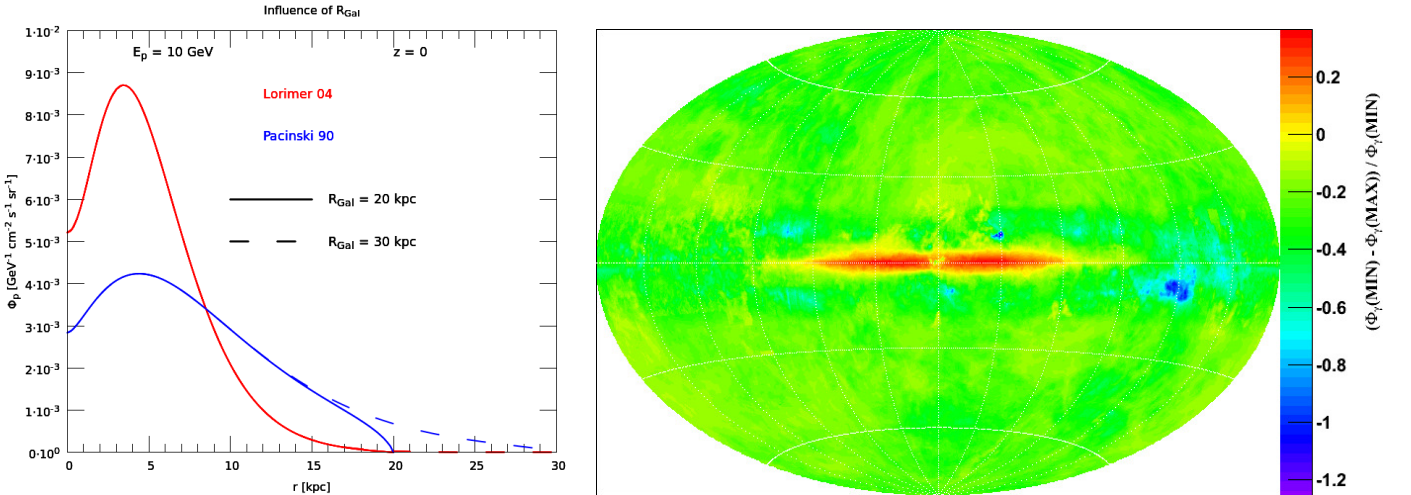

Fig. 9. The influence of the radial boundary R_{Gal} of the DH on the Galactic γ-ray diffuse emission: In the left panel, the CR proton radial distribution along the Galactic disk – also called the CR proton gradient – is displayed for a radial boundary R_{Gal} of 20 kpc (continuous line) and 30 kpc (dashed line), for the two source profiles L04 in red (Lorimer 2004) and P90 in blue (Paczynski 1990). In the right panel, we have plotted the ratio (map2 − map1)/map1 for each pixel where map1 and map2 were derived with $R_{Gal} = 20$ and 30 kpc respectively. The CR source profile is P90 here, all the other inputs being the same as in the reference map of Fig. 1.

The radial extension of the DH is the last propagation parameter whose effect on the Galactic γ-ray diffuse emission needs to be explored. In previous studies, we always considered R_{Gal} to be 20 kpc, because CR data at the Earth are not very sensitive to this value. However, when considering γ-rays, some variations can appear when changing the value of this parameter. As illustrated in

the right panel of Fig. 9, changing $R_{\rm Gal}$ from 20 to 30 kpc induces up to a 6% increase in the γ-ray flux from the anti-center region. However, this result strongly depends on the source distribution profile $\rho(r, 0)$ considered. Indeed, as shown in the left panel, if we take the source profile L04 of Lorimer (2004) (see section 4.3 and Fig. 12 for more details), then almost no variation comes from the increase of $R_{\rm Gal}$. This profile gives an almost null source density at large Galactic radii. On the contrary, the source distribution P90 from Paczynski (1990) features a non-negligible amount of sources beyond a Galactocentric distance of 20 kpc, hence a moderate increase in the γ-ray flux from the anti-center region. We would like to stress that large uncertainties exist concerning the distribution of supernova remnants at large Galactic radii. The effect of increasing $R_{\rm Gal}$ could then be stronger than what has been derived here with the P90 profile.

4. Other sources of uncertainties

In this section, we discuss first the effect of the γ-ray production cross section and then of the injection CR proton et helium fluxes on the effective emissivity at the Earth $\mathcal{E}_{\rm eff}(\odot)$ of the ISM. We would like to disentangle the potential sources of uncertainties that are likely to affect the γ-ray flux. That is why the discussion of sections 4.1 and 4.2 focuses on $\mathcal{E}_{\rm eff}$ and not on Φ_γ. CR Galactic propagation is involved in section 4.3 where we analyze how various choices for the Galactic distribution of primary CR sources influence our predictions.

4.1. Gamma-ray production cross section

Most of the recent calculations of the fluxes at the Earth of secondary CR leptons (see for instance Delahaye et al. 2009; Delahaye et al. 2010) are based on the Kamae et al. (2006) parameterization of the production cross sections in proton-proton collisions. The inclusive pion production cross section is drawn from Blattnig et al. (2000). Older works – in particular the article by Moskalenko & Strong (1998) which has led to the GALPROP package – make use of the Badhwar et al. (1977) parameterization. The short-dashed magenta curve of Fig. 10 has been derived with the Kamae et al. (2006) parameterization and the Shikaze et al. (2007) measurements of the proton flux at the Earth. This curve features the partial γ-ray emissivity $\mathcal{E}_{\rm pH}$ for which only proton-proton interactions have been taken into account. It lies well below the other lines for which the contributions of nuclear collisions have been included.
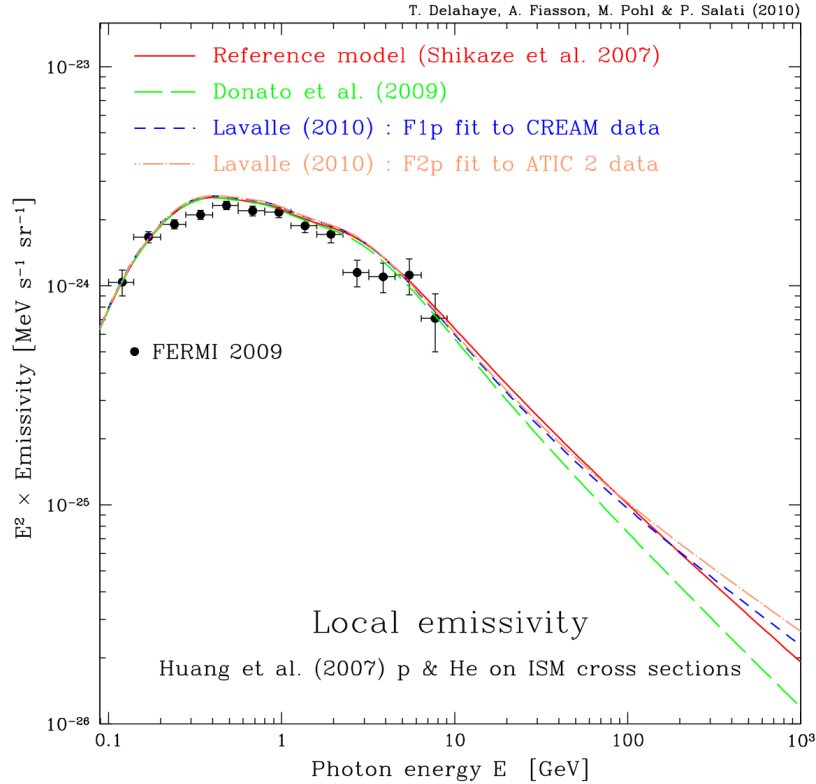

Fig. 10. The local effective emissivity $\mathcal{E}_{\rm eff}$ of the ISM per hydrogen atom recently measured (Abdo et al. 2009) by the Fermi collaboration. The black data points are plotted with various predictions based on different γ-ray production cross sections. The red solid curve features our reference model for which the Huang et al. (2007) cross sections are combined with the Shikaze et al. (2007) proton and helium fluxes. The magenta short-dashed curve is the emissivity for only proton-proton interactions and is based on the Kamae et al. (2006) parameterization. Taking then into account the nuclear weight factors of eqs. 28 and 27 yields the blue and orange long-dashed curves. In all cases, the cross sections are convoluted with the CR proton and helium fluxes measured at the Earth's position by Shikaze et al. (2007).

The production of a γ-ray – and of any species for that matter – by a CR nucleus A_i impinging on a target nucleus A_t of the ISM is modeled through the nuclear weight factor w defined as

$$\frac{d\sigma}{dE}(A_i[T] + A_t \to \gamma[E]) = w(A_i, A_t, T, E) \times \frac{d\sigma}{dE}(p[T] + H \to \gamma[E]) \ . \tag{26}$$

The weight w gauges the nuclear effects involved in the γ-ray production during a nucleus-nucleus interaction and scales them with respect to the equivalent proton-proton collision. It depends on the atomic numbers A_i and A_t of the projectile and target nuclei. Its variations with the energy E of the photon and the kinetic energy per nucleon T of the CR nucleus are in general disregarded. A nucleus-nucleus collision can be naively understood as a collection of nucleon-nucleon interactions where protons and neutrons have identical behaviors. Relation (26) is based on this scheme and w accounts for the number of two body reactions occurring during a nuclear collision. Various prescriptions have been proposed in the literature such as the Orth & Buffington (1976) formula

$$w_{\mathrm{OB}} = \left(A_i^{3/8} + A_t^{3/8} - 1 \right)^2 \ , \tag{27}$$

or the more recent Norbury & Townsend (2007) scaling factor

$$w_{\mathrm{NT}} = (A_i A_t)^{0.8} \ . \tag{28}$$

Both prescriptions have been combined with the Kamae et al. (2006) proton-proton cross section and the Shikaze et al. (2007) proton and helium fluxes to yield the long-dashed dotted orange (KOB) and the long-dashed blue (KNT) curves, which are close to. The Orth & Buffington (1976) nuclear weight leads to a result that is slightly smaller than the Norbury & Townsend (2007) prediction. The KOB and KNT models actually differ by less than 3.7% for a photon energy E in the range extending from 100 MeV to 1 TeV. The red curve corresponds to our reference model. The emissivity has been obtained by combining the Huang et al. (2007) cross sections with the Shikaze et al. (2007) proton and helium fluxes. The result is significantly higher than for the KNT or KOB models, with a difference of about 33% at 1 GeV, which reaches a maximum of 54% at 4.5 GeV and decreases down to 20 to 30 % above 100 GeV. Because the Huang et al. (2007) parameterization is based on the Kamae et al. (2006) proton-proton cross section at low proton energy, our reference model is quite close to the KNT or KOB predictions at low photon energy. The difference is only 13% at 100 MeV. At high energy, the DPMJET-III code incorporates the direct production of photons, a process which is not included in the Kamae et al. (2006) parameterization. Nuclear reactions are also modeled more accurately.

In the literature, the nuclear effects are often described by the nuclear enhancement factor ϵ_M, which is defined as the ratio

$$\epsilon_M = \mathcal{E}_{\mathrm{eff}}(\mathbf{x}, E)/\mathcal{E}_{\mathrm{pH}}(\mathbf{x}, E) \ . \tag{29}$$

This factor depends a priori on the photon energy E and on position $\mathbf{x}$ within the CR diffusive halo. Even though the various nuclear weight factors w may only depend on the atomic numbers of the projectile and target nuclei, the CR helium and proton fluxes do not undergo the same variations as the kinetic energy per nucleon T and the position $\mathbf{x}$ are changed. We calculated ϵ_M in the KNT model and mapped its variations inside the CR diffusive halo for different photon energies. We find that ϵ_M is basically constant. At the sun position, it decreases from 1.544 at 1 GeV down to 1.526 at 100 GeV. Throughout the CR diffusive halo, ϵ_M varies by a factor of 2.4% at 1 GeV. The amplitude of the spatial variations decreases to only 0.15% at 100 GeV. We find similar results for the KOB model, with a solar value of ϵ_M decreasing from 1.491 at 1 GeV down to 1.475 at 100 GeV. A good estimate of the nuclear enhancement factor is therefore given by its local value. Assuming that relations (27) or (28) hold leads to the approximate expression

$$\epsilon_M = \sum_{\mathrm{A}} \frac{X_{\mathrm{A}}}{X_{\mathrm{H}}} \left\{ w(1, \mathrm{A}) + w(4, \mathrm{A}) \frac{\Phi_\alpha(\odot)}{\Phi_p(\odot)} \right\} \ , \tag{30}$$

where the helium to proton CR flux ratio at the Earth has been taken as constant. This is not quite correct actually. Because the Shikaze et al. (2007) spectral indices for CR proton and helium nuclei are equal to 2.76 and 2.78 respectively, we get a small decrease of ϵ_M with energy. The element abundances in the ISM also matter. If we adopt the solar value of 0.0975 for the $X_{\mathrm{He}}/X_{\mathrm{H}}$ ratio instead of the interstellar canonical value of 0.111, the KNT nuclear enhancement factor decreases by 3% and is now very close to the KOB value.

The predictions of the KNT and KOB models at 10 GeV – respectively 1.535 and 1.483 – are in very good agreement with the value of 1.52 found by Gaisser & Schaefer (1992). Since that publication, the modeling of nuclear interactions has been considerably improved thanks in particular to the DPMJET event generator. But because the Huang et al. (2007) parameterization is given for proton and helium nuclei interactions with the ISM taken as a whole, the nuclear enhancement factor ϵ_M cannot be extracted. We had no access to the Huang et al. (2007) proton-proton cross section and could not compute $\mathcal{E}_{\mathrm{pH}}$. To get a feeling for how large ϵ_M can be in that case, we used the nuclear weight factors w that Mori (2009) calculated with the DPMJET-III Monte Carlo code and we combined them with the Kamae et al. (2006) proton-proton cross section and the same ISM composition as in Huang et al. (2007). At 10 GeV, we derive a value of 1.69, well above the KNT or KOB predictions. Mori (2009) finds a nuclear enhancement factor as large as 1.84 at 10 GeV, increasing up to 2.00 at 1 TeV. In his analysis, nuclei up to Fe are included in both the ISM and the CR projectiles. The parameterization of the various CR fluxes is also borrowed from Honda et al. (2004) whereas our estimate of ϵ_M relies on the Shikaze et al. (2007) measurements. The CR helium-to-proton flux ratio increases like $T^{0.1}$ in the former case, whereas it decreases slightly in our case. We never made use of this nuclear enhancement factor ϵ_M because our calculations are based directly on γ-ray production cross-sections, nuclear weight factors w, and the CR proton and helium fluxes measured at the Earth.

4.2. Cosmic ray proton and helium fluxes at the Earth

The fluxes at the Earth of CR protons and helium nuclei actually do matter in calculating $\mathcal{E}_{\text{eff}}$. In Fig. 11, the Huang et al. (2007) cross sections have been combined with a selection of different parameterizations to yield the ISM effective emissivity at the solar circle. The red solid curve stands for our reference model based on the Shikaze et al. (2007) proton and helium fluxes. It extends up to 1 TeV the corresponding curve of Fig. 10. Because hadronic interactions are basically scale invariant, the emissivity decreases with roughly the same spectral index as the progenitor CR proton and helium fluxes. The latter have been parameterized by Shikaze et al. (2007) with the simple power law

$$\Phi = A \, \beta^{p_1} \, \mathcal{R}^{-p_2} \quad \text{cm}^{-2} \, \text{s}^{-1} \, \text{sr}^{-1} \, (\text{GeV/n})^{-1} \ , \tag{31}$$

where $\mathcal{R}$ denotes the rigidity of the nucleus expressed in units of GV. The Shikaze et al. (2007) measurements yield the parameterizations $(A, p_1, p_2) = (1.94, 0.7, 2.76)$ for H and $(0.71, 0.5, 2.78)$ for He. Between 3 GeV and 1 TeV, our reference model leads to an emissivity approximated well by

$$\mathcal{E}_{\text{eff}}(\odot, E) \simeq 3.55 \times 10^{-27} \, \text{GeV}^{-1} \, \text{s}^{-1} \, \text{sr}^{-1} \left(\frac{1 \, \text{GeV}}{E} \right)^{2.76} \ . \tag{32}$$
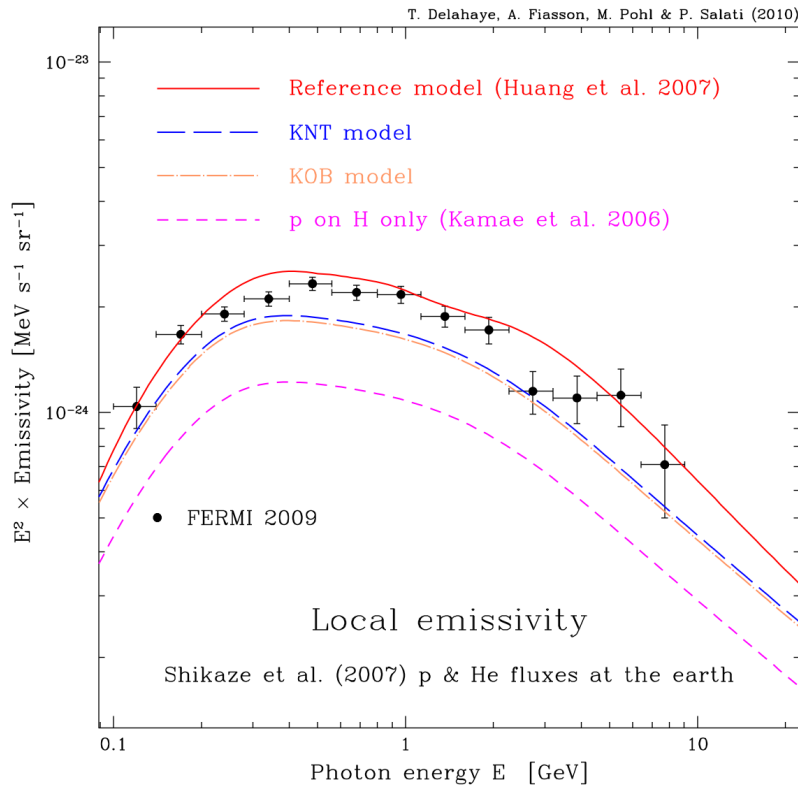

Fig. 11. The measurements by Abdo et al. (2009) of the local effective emissivity $\mathcal{E}_{\text{eff}}$ of the ISM per hydrogen atom (black data points) are compared to various predictions for which the Huang et al. (2007) cross sections have been used. A selection of different parameterizations for the CR proton and helium fluxes at the Earth is featured. The curves diverge from each other above 10 GeV and the spread among them reaches a factor of 2 at 1 TeV.

A crucial element in the calculation of the Galactic diffuse γ-ray emission is the interstellar (IS) fluxes of protons and helium nuclei. These fluxes are actually measured at the top of the terrestrial atmosphere (TOA) and have been considerably altered during their journey through the heliosphere. As pointed out by Donato et al. (2009), determination of the spectral indices of the IS fluxes from their TOA values is potentially spoilt by solar modulation. The latter tends to harden the spectra even beyond 10 GeV/n so that only the highest energy points should be used to parameterize the IS fluxes. Unfortunately, these points are most subject to statistical uncertainties as the CR fluxes decrease at high energy where very few events are collected. CR measurements with large detectors will ensure in the future substantial statistics and will help determine the IS high-energy spectra with improved accuracy. To gauge this effect, we used the Donato et al. (2009) parameterizations, which are borrowed from Shikaze et al. (2007) below 20 GeV/n and are otherwise given by $(A, p_1, p_2) = (2.4132, 0, 2.839)$ for H and $(0.8866, 0, 2.85)$ for He. This yields the curve that departs from the red solid line above 10 GeV and is a factor 0.62 below it at 1 TeV.

The balloon experiments ATIC2 (Panov et al. 2009) and CREAM (Ahn et al. 2010) have recently reported a significant hardening of the proton and helium spectra above 200 GeV/n. Although both experiments agree on the helium spectrum, ATIC2 finds a larger

proton excess than CREAM. These new fluxes have been parameterized by Lavalle (2010) and lead to those two other curves. The former is based on the Lavalle (2010) F1p fit to the proton data measured by CREAM, while the latter makes use of the F2p fit to the ATIC2 proton flux. Once again, the various emissivities show similar behaviors below 10 GeV. Up to 100 GeV, the F1p and F2p predictions are below the reference model whose parameterization of the proton and helium fluxes does not reproduce the dip observed in the ATIC2 and CREAM data well. Above 100 to 200 GeV, the F1p and F2p emissivities overreach the reference model by a factor respectively equal to 1.19 and 1.37 at 1 TeV. This is comparable to the increase of about 30% found by Donato & Serpico (2011) for photons at energies close to 300 GeV.

4.3. Distribution of the primary cosmic ray sources in the disk

Though convincing proof remains to be given, it is widely accepted that the main source of CR proton and α particles in the GeV-TeV energy range are the supernova remnants. Indeed there are more and more observational hints pointing towards supernova remnants – see for instance Feinstein et al. (2009). From the theoretical point of view, these objects are the perfect location for Fermi acceleration. However, supernova remnants are very difficult to detect because as they get older, they expand hence become dimmer and dimmer, so that even nearby ones are difficult to see because they sometimes become so big in the sky that they exceed the angular acceptance of the radio telescopes. The most up-to-date catalog (Green 2009) contains only 274 objects and the precise location of most of them is unknown. However, as two thirds of the supernovæ are expected to have undergone core collapse, one can use pulsars as tracers of the supernova remnants distribution. The ATNF catalog[1] (Manchester et al. 2005) lists more than 1800 pulsars. Nevertheless, too naive use of the statistics would lead to errors, since it is well known that data do not reflect reality faithfully because of detection biases (e.g. Lorimer 2004).
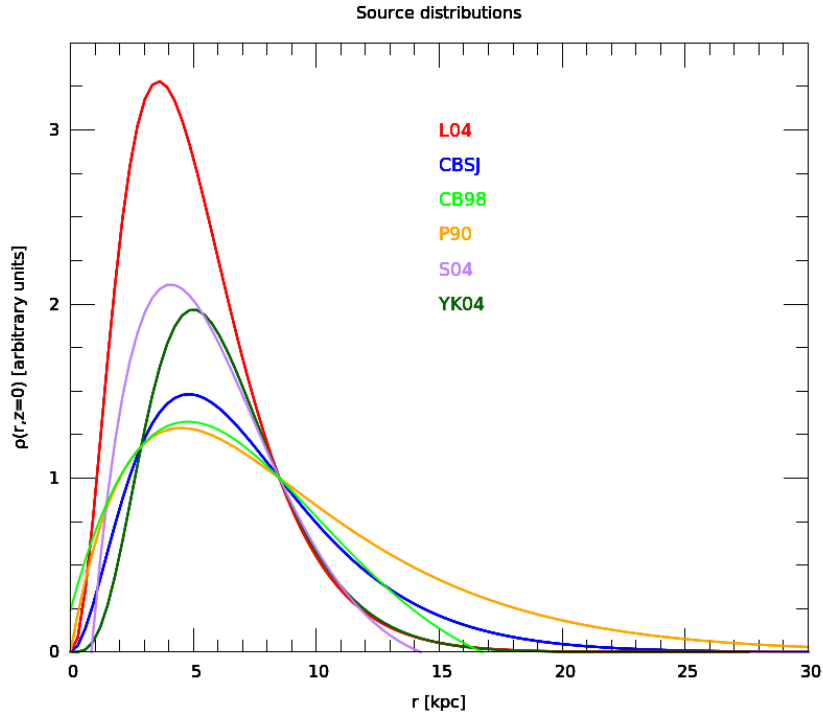

Fig. 12. Various cosmic ray source (supernova remnants) distributions are available in the literature. They are plotted here as a function of the Galactocentric distance r. The references of the curves are Lorimer (2004) in red (L04), Case & Bhattacharya (1998) in blue (CBSJ), Case & Bhattacharya (1998) in light green (CB98), Paczynski (1990) in orange (P90), Sasaki & Breitschwerdt (2003) in purple (S04) and Yusifov & Küçük (2004) in dark green (YK04). For clarity, all these distributions have been normalized here with respect to their solar circle values. However, this is not what is used in our calculations since the normalization of the CR production rates are set automatically by the *retropropagation* method explained in section 2.2.

There are few distribution models in the literature that we can compare. Most of them exhibit radial dependencies in the form proposed by Stecker & Jones (1977) with

$$\rho(r,z) = \rho_0 \times r^a \times \exp\left\{-\frac{r}{r_0}\right\} \; , \tag{33}$$

---
[1] http://www.atnf.csiro.au/research/pulsar/psrcat

where ρ_0 is the normalization[2] and r the distance from the Galactic center. Having made use of the thin disk approximation to describe the Galactic plane, we have not considered any vertical variation of these profiles. Different sets of values can be found in the literature for the pair of parameters (a, r_0). Lorimer (2004), hereafter L04, found (2.35 , 1.528 kpc) and Yusifov & Küçük (2004), hereafter YK04, derived (4 , 1.25 kpc). Case & Bhattacharya (1998), hereafter CBSJ, got (2.0 , 3.53 kpc) while Paczynski (1990), hereafter P90, determined (1 , 4.5 kpc). Finally, at variance with the parameterization sketched above, we mention the distribution proposed by Case & Bhattacharya (1998) and denoted hereafter CB98. Though obtained from a fit performed on a poor statistical ensemble of only 36 supernova remnants, that profile has the particularity of giving a non zero density at the Galactic center since

$$\rho(r, 0) = \rho_0 \times \sin\left(\pi\frac{r}{r_s} + \theta\right) \times \exp\left\{-\frac{r}{r_0}\right\} \quad . \tag{34}$$

The authors find that $r_0 = 7.7 \pm 4.7$ kpc, $r_s = 17.2 \pm 1.9$ kpc and $\theta = 0.08 \pm 0.33$. This relation is only valid as long as $r \leq r_s \times (1 - \theta/\pi)$ (*i.e.* in the inner 16.8 kpc) and is zero beyond. All these distributions are displayed in Fig. 12. Brogan et al. (2006) have recently reported the detection of 35 new supernova remnants in the inner Galaxy and suggest that earlier radial distribution estimations should be revised.
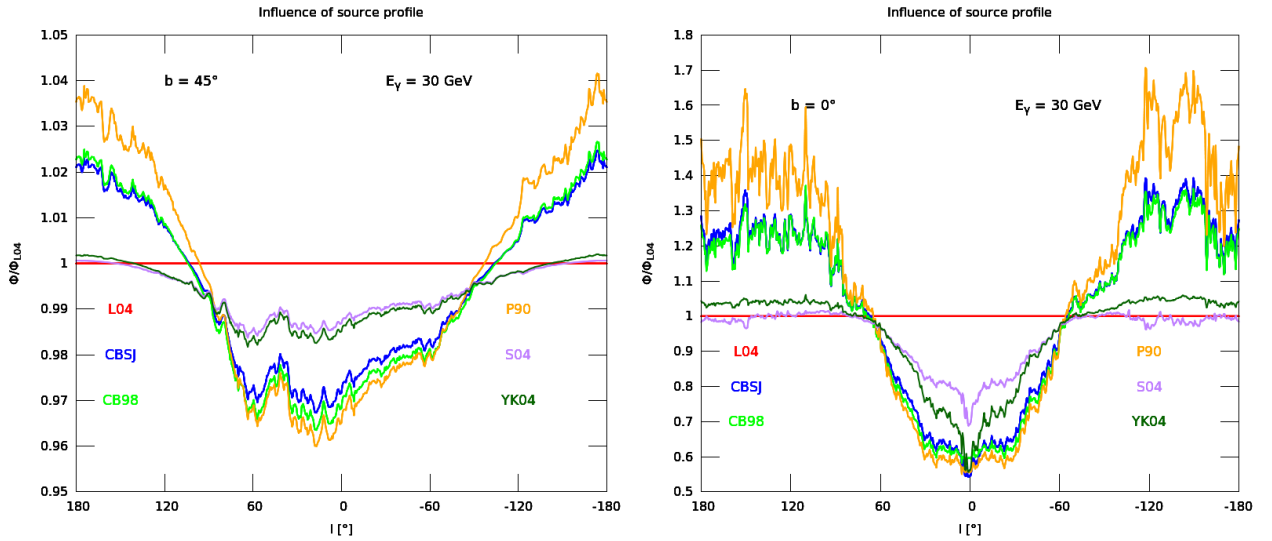

Fig. 13. Variations in the γ-ray flux as a function of the Galactic longitude l relative to the reference model L04 of Fig. 1. All the source distributions described in section 4.3 are displayed. The left panel corresponds to the Galactic disk with a latitude b of $0°$, whereas the right panel features the case of the intermediate latitude $b = 45°$.

As is clear from Fig. 12, there are large variations from one model to another. The position and the magnitude of the peak of the supernova remnant distribution varies from one author to another. Even more striking, far away from the Galactic center, for a distance r greater than 12 kpc, the distributions are very different. For instance, the CB98 profile has no source beyond 17 kpc, whereas in the P90 case, the source distribution extends far away beyond 20 kpc. As already mentioned in section 3 and evoked in the right panel of Fig. 9, the differences in the radial profiles of the primary CR sources from one author to another imply large variations in the expected γ-ray flux in the anti-center direction. As illustrated in Fig. 13, the uncertainties on the γ-ray diffuse emission due to the CR source distribution can be as large as 70% towards the Galactic anti-center and reach up to 50% in the direction of the Galactic center. However, because diffusion is quite efficient, the memory of the source distribution in the cosmic ray gradient is erased quite quickly away from the Galactic plane. Indeed, at the latitude b of $45°$ presented in the right panel of Fig. 13, the uncertainties only decrease to 4%.

5. The distribution of hydrogen in the Galaxy

The hydrogen density $n_H(\mathbf{x})$ is a key ingredient in calculating the γ-ray diffuse emission flux Φ_γ. Each hydrogen atom nucleus or proton of the ISM that lies inside the DH is embedded inside radiations of cosmic protons and α particles, and shines in the γ-ray band. Determining the Galactic distribution of hydrogen with accuracy is therefore paramount. This distribution falls into three distinct parts of unequal importance. Atomic neutral hydrogen HI is directly traced through its 21-cm line emission. It has been mapped all over the sky and an up-to-date survey is provided by the Kalberla et al. (2005) catalog. Molecular hydrogen is the dominant component inside the Galactic disk. It acts as a coolant that triggers gas collapse and stellar formation. It cannot be detected directly but its presence is traced by molecules, such as CO, which are associated to stellar activity. The most up-to-date map is the composite CO survey by Dame et al. (2001). Finally, ionized hydrogen HII has been included in our calculations, although it is an inessential component.

---

[2] This normalization is not very important for us as our *retropropagation* method automatically sets the magnitude of the CR Galactic production rates Q_{tot} in order to ensure the correct CR fluxes at the Earth.

5.1. The hydrogen 3D distribution of this analysis

We used here the results of Pohl et al. (2008), who have kinematically deconvolved the composite Dame et al. (2001) CO survey with a gas-flow model derived from smoothed particle hydrodynamics (SPH) simulations in gravitational potentials based on the NIR luminosity distribution of the bulge and disk (Bissantz et al. 2003). Besides providing a more accurate picture of cloud orbits in the inner Galaxy, a fundamental advantage of this model is that it provides kinematic resolution towards the Galactic center, in contrast to standard deconvolution techniques based on purely circular rotation. The same technique was applied to deconvolve the LAB HI survey (Kalberla et al. 2005) with appropriate modifications reflecting the larger single-cloud linewidth and the galactic warp and flaring in the outer Galaxy (Kalberla & Kerp 2009). The kinematic deconvolution is applied only in the Galactic plane, whereas both the CO and HI data are distance-allocated according to scale height at $|b| > 5°$ and $|b| > 10°$, respectively. Any kinematic deconvolution suffers from systematic errors, and artifacts may appear in the final maps. For example, in some regions line signal is observed at atypical velocity for some reason, which the code would allocate in distance according to the global flow model. It is rare that such features dominate the gas maps, but we cannot exclude that some peaks in the difference map (see Fig. 2) are enhanced by these systematic effects.

No systematic correction is made for HI absorption or self-absorption. The former is potentially important in areas of high 21-cm continuum intensity, and we have indeed interpolated (in l, b) the spectra towards the Galactic center or Cas A to correct negative spikes, but a general and systematic correction would very much depend on the assumed hydrogen spin temperature (Dickey et al. 2003). HI self-absorption arises from cold clouds located in front of warmer hydrogen and is generally a small-scale feature that may be expected to be washed out when considering large-scale features (Gibson et al. 2000).

5.2. The GALPROP gas maps

Based on the surveys of Kalberla et al. (2005) for HI and Dame et al. (2001) for CO, and making use of various models for the rotational curves of the Galaxy, which are detailed in the appendix of Moskalenko et al. (2002), Seth W. Digel built a gas distribution map for the GALPROP package (Strong & Moskalenko 1998), which is available online. This model is based on a cylindrical symmetry (the Galaxy is described as 8 annuli) and does not take the spiral arm structure of the Milky Way into account.
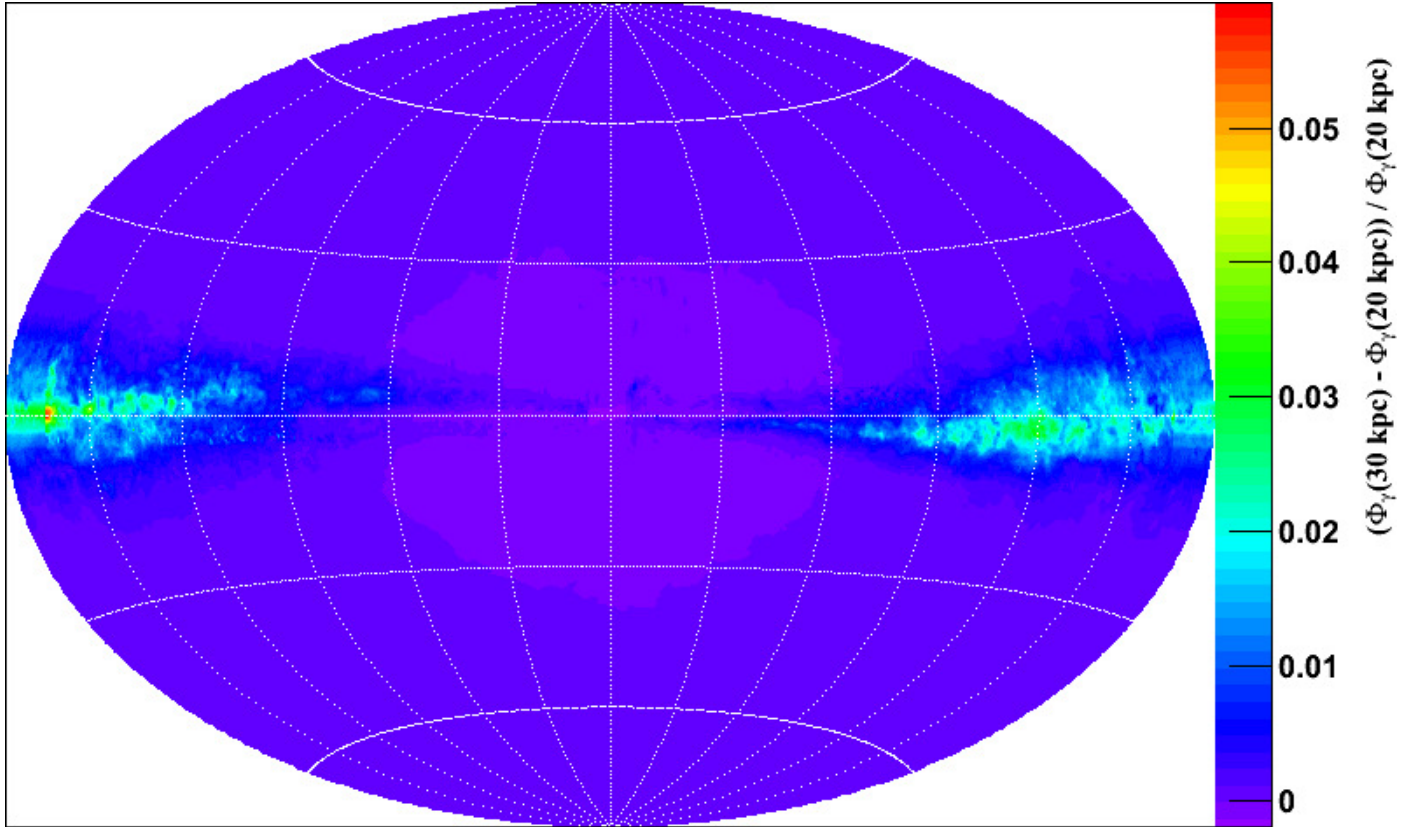

Fig. 14. Relative variations in the Galactic γ-ray diffuse emission with respect to the reference case of Fig. 1. We have plotted here the ratio (map1 − map2)/map1 where map1 is our reference map whereas map2 was obtained from the hydrogen distribution available in the GALPROP package with all the other inputs the same as for map1. In particular, the photon energy is 30 GeV.

Fig. 14 displays the relative variations in the γ-ray flux when using the GALPROP gas maps instead of the Pohl et al. (2008) distributions. In order to disentangle the effect of the actual 3D gas distribution from the influence of the X_{CO} factor, which will be discussed in the next section, we took a constant value for the latter (as in the original GALPROP work). Also, we have not

compared the output from the GALPROP routine to our γ-ray flux here. We have merely incorporated the GALPROP hydrogen maps in our calculations to assess the influence of the sole Galactic gas distribution. We therefore prepared a γ-ray sky map in exactly the same conditions as for the reference map of Fig. 1 except for the hydrogen density, which was borrowed from the GALPROP package. The relative differences between the GALPROP-inspired map (map2) and our reference case (map1) have been plotted in Fig. 14, which clearly points toward strong contrasts. The blue spots below the Galactic plane are caused by different treatments of the Magellanic Clouds and Messier 31. Some pixels have values higher than unity because the map computed with the GALPROP gas distribution unexpectedly leads to negative results in some directions. The other structures that appear are probably caused by the annular structure of the GALPROP gas map. Finally, on top of the CO maps, an inspection of Fig. 14 at high Galactic latitude indicates that the HI maps are also quite different. Taking the spiral arm structure of the Milky Way into account is extremely important and has a strong effect on the predictions of the Galactic γ-ray diffuse emission.

5.3. The X_{CO} factor

Most of hydrogen gas in the Galactic plane is under the molecular form H_2. However, directly measuring its column density is extremely difficult as this molecule is homopolar. It does not shine in the infrared where its spectroscopy is rather poor. Conditions in molecular clouds are furthermore unsuitable for the rotational transitions of H_2. Carbon monoxide (CO), the most abundant component of interstellar gas after H_2 and the almost undetectable helium, has a non vanishing dipole moment with rotational transitions which are easily excited under molecular cloud conditions. The question is then to determine the relative abundance of H_2 with respect to CO. The observed CO intensity, expressed as an integrated brightness temperature, is denoted by W_{CO} and expressed in units of K km s^{-1}. The H_2 column density is then expressed as

$$N(H_2) \equiv \int_{los} ds\, n_{H_2} = X_{CO} \times W_{CO} \,, \tag{35}$$

where X_{CO} is the conversion factor. Our reference model is based on the value of 2.3×10^{20} molecules cm^{-2} (K km s^{-1})$^{-1}$, see for instance Strong et al. (1988) or Bertsch et al. (1993), which we took as constant throughout the Galaxy. However, as explained by Glover & Mac Low (2010) and Shetty et al. (2010) who uses hydrodynamical simulations, H_2 and CO formation follows different mechanisms. H_2 formation is mainly ruled by the time available to the gas cloud whereas CO formation highly depends on the carbon and oxygen abundances (metallicity) and the strength of the background ultraviolet (UV) radiation field that dissociates CO molecules. These authors have shown that X_{CO} may vary from 0.9 to 5×10^{20} molecules cm^{-2} (K km s^{-1})$^{-1}$ and even over one order of magnitude in extreme molecular cloud conditions. Because metallicity and UV radiation field are not homogeneous in our Galaxy, it is even expected that the X_{CO} factor has a spatial dependence. As a result, we compared our reference model to the various radial profiles of the X_{CO} factor, which can be found in the literature. In Fig. 15, following Strong et al. (2004), we used the profiles given by Sodroski et al. (1995) and by Sodroski et al. (1997), as well as the profiles that those authors inferred from Israel (1997) and Boselli et al. (2002). We moreover used the X_{CO} radial profile, which can be found in the GALPROP package. We finally implemented the recent studies by Nakanishi & Sofue (2006) and modified the GALPROP function according to the studies of Tibaldo et al. (2009) for the second quadrant and Tibaldo et al. (2010) for the third one. All these profiles are displayed in the left panel of Fig. 15.
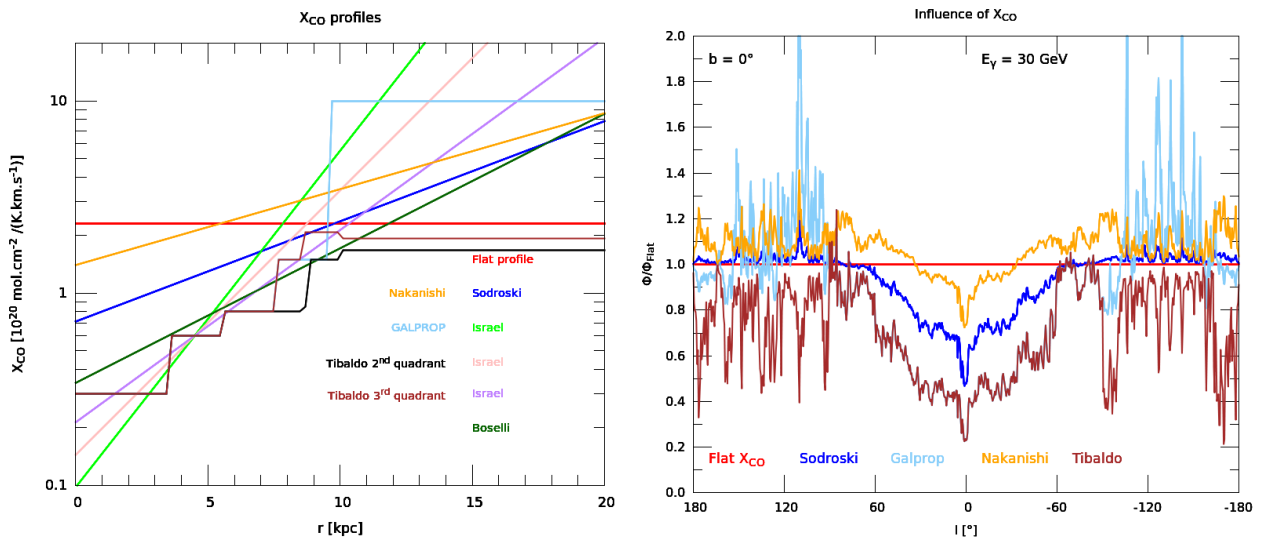

Fig. 15. The various X_{CO} Galactic radial profiles available in the literature are displayed in the left panel. The corresponding variations in the γ-ray flux at 30 GeV and $b = 0°$ are displayed relative to our reference model of Fig. 1 for which the constant value of 2.3×10^{20} molecules cm^{-2} (K.km.s^{-1})$^{-1}$ has been assumed for X_{CO}. The three (cyan) peaks, whose maxima have not been displayed for clarity, reach a value of 3.0, 2.3, and 2.3 respectively from left to right.

As featured in the right panel of Fig. 15, which concentrates on the Galactic plane, the variations in the γ-ray flux, induced by a change in the X_{CO} factor with respect to our reference value of 2.3×10^{20} molecules cm^{-2} (K km s^{-1})$^{-1}$, are very important and may reach up to 200%. This is probably the largest source of uncertainty in this work. At higher latitudes, where atomic hydrogen HI starts to dominate molecular hydrogen H_2 – however the CO survey by Dame et al. (2001) is at that time only fragmentary as it covers the limited band in latitude $-30° \leq b \leq 30°$ – the uncertainties due to the X_{CO} factor drop very fast. Moreover, one should stress that only the radial variations of X_{CO} have been considered here, although we expect the UV radiation field to vary with the distance $|z|$ to the Galactic plane. So should X_{CO}, but no description of this effect has been published so far.

In the recent years some observations have led to the conclusions (Grenier et al. 2005; Abdo et al. 2010; Planck Collaboration et al. 2011) that not only the CO to H_2 relation is not completely understood but even worse, both gas distributions are sometimes uncorrelated: indeed there are molecular clouds of *dark gas* that contain copious amounts of molecular hydrogene but no CO at all. The precise amount of *dark gas* in the Galaxy is not known yet, and there is no way to take it into account in this study, hence another source of uncertainties that can be quite large, especially in the direction of the Galactic anti-center.

6. Conclusions

In this article, we have explored various sources of uncertainty that affect any determination of the hadronic component of the Galactic γ-ray diffuse emission in the GeV-TeV range. To do so, we used the Maurin et al. (2001) semi-analytic two-zone Galactic CR propagation model. The derivation of the densities of CR protons and helium nuclei everywhere inside the Galactic DH is immediate once the spectra of these species have been measured at the Earth. Our method allows therefore a rapid calculation of the γ-ray flux and a minute of CPU time is enough to get, on an ordinary PC, a full sky map at the precision of half a degree both in latitude and longitude. We devised an efficient tool with which we investigated several potential sources of uncertainty and we quantified the corresponding errors on the γ-ray flux. These are more or less important depending on the process at work. Most of them – but not all of them – are likely to be considerably reduced in the future when better data are available.

To commence, the uncertainties on the γ-ray flux that arise from a particular choice for the photon production cross sections and the primary CR proton and helium fluxes are gauged by the spread of the various curves presented in Figs. 10 and 11. In the case of cross sections, the uncertainty is featured by the band lying between the long-dashed blue (KNT) and red solid (reference) curves of Fig. 10. It increases from 13% at 100 MeV up to a maximum of 54% at 4.5 GeV. It then decreases down to 20% at 60 GeV to reach a plateau of 30% at 1 TeV. We also showed that the proton and helium fluxes at the Earth's position are key inputs in the calculation of the γ-ray flux. A better determination of the spectra of these species at high energy would be invaluable. Given the current observations, our reference model prediction could be varied by $\pm$ 40% at 1 TeV. A better understanding of the nuclear processes at stake and refined measurements of the proton and helium spectra at high-energy are therefore mandatory in order to calculate more reliably the Galactic γ-ray diffuse emission. There is actually matter for some hope: colliders like the LHC will soon explore proton-proton and nucleus-nucleus interactions at unprecedented energies. The photon production cross sections of these processes are likely to be better parameterized in the future leading to improvement in our understanding of the mechanisms at work. The CR proton and helium fluxes at the Earth will also be soon measured with much better accuracy by experiments like AMS02 (Incagli 2010) or CREAM (Ahn et al. 2010).

We then found that the normalization K_0 and the spectral index δ of the space diffusion coefficient K have little influence on the γ-ray flux, especially at high energies. This surprising result can be understood easily. The transport of high-energy CR protons and α particles inside the Galactic DH is dominated by space diffusion. In this regime, the densities of these species are merely proportional to the ratio of the Galactic production rates Q_{tot} to the diffusion coefficient K. Once the CR proton and helium fluxes at the Earth are fixed, a variation in K translates into the same variation in Q_{tot}. The distribution of CR protons and helium nuclei throughout the DH remains unaffected. So does the γ-ray diffuse emission. What actually matters is the competition between convection and diffusion. When convection is taken into account, with a nonvanishing value for the wind V_C, CR primaries are washed away from the Galactic plane as they diffuse from the molecular ring to the Earth. Their densities are no longer proportional to the ratio Q_{tot}/K. At fixed proton and helium densities at the Earth, an increase in V_C with respect to K translates into brighter sources and above all into a denser population of CR primaries around the molecular ring. The γ-ray diffuse emission becomes brighter towards the Galactic center. It also fades in the direction of the anti-center where the cosmic ray gradient steepens. Finally, a change in K or V_C only has a moderate effect on Φ_γ. Even at sub-GeV energies where the competition between convection and diffusion is significant, the effect does not exceed 10%.

We also explored how the size of the DH could affect the photon flux. A radial extension of the DH has a zero-to-moderate effect depending on the population of supernova remnants at large Galactocentric distances. Even in the case of the P90 profile and its substantial amount of sources beyond a radius of 20 kpc, the effect does not exceed 6% as shown in the right panel of Fig. 9. The γ-ray diffuse emission is not at all affected if the L04 profile is now chosen. This is not the case when the thickness of the DH is varied. The latter acts as a reservoir inside which the hydrogen is illuminated by CR protons and α particles. An increase in L translates directly into a larger abundance of gas with which CR primaries can interact and hence into a larger photon flux. The effect is significant as illustrated in Fig. 8 with a variation of -30% to $+12\%$ around the reference value of the MED model. This situation is likely to be remedied in the future. Better B/C data should help for improving the determinations of the K/L ratio and of the spectral index δ as discussed in Castellina & Donato (2005). Accurate measurements of the ^{10}Be/^{9}Be ratio would then help lift the degeneracy between L and K. Once again, there is matter for some hope with forthcoming experiments like AMS02 (Incagli 2010) or CREAM (Ahn et al. 2010).

This may not be the case for the distribution of primary CR sources along the Galactic plane. The radial profile of supernova remnants indeed has a significant effect on the γ-ray diffuse emission with variations as large as 50% towards the Galactic center and 70% in the opposite direction. As long as the primary CR source distribution is not determined better, the γ-ray flux will be affected

by a large uncertainty. Radio surveys and observations (by the Fermi or HESS collaborations for instance) of active sources should shed some light on that problem. Interestingly enough, our results are insensitive to the different source profiles at a longitude of about $\pm 60°$ as indicated in the left panel of Fig. 13.

We finally showed that the γ-ray diffuse emission is extremely sensitive to the Galactic spatial hydrogen distribution. As expected, predictions depend significantly on the HI and CO maps in three dimensions, as well as on the assumptions on the X_{CO} conversion factor. Inside the red regions of Fig. 14, our prediction is twice as large as that of GALPROP. The γ-ray diffuse emission is actually a probe of the gas distribution inside the Milky Way and offers a unique tool for measuring the density of hydrogen along the line of sight, hence an extreme sensitivity to n_H. For this tool to work efficiently, all the other sources of uncertainty need to be reduced. Much effort should be put into a better determination of the thickness of the DH and the supernova remnant radial profile.

Our conclusions on the effects of CR propagation are qualitatively comparable to the results of Cumberbatch et al. (2010) although a quantitative comparison is not possible. These authors have concentrated on a small region in latitude with $10° \leq |b| \leq 20°$ and not on the entire sky. They vary the half-depth L of the DH from 4 to 11 kpc. This range is more limited than ours. They have above all explored energies as low as 20 MeV and incorporated into the γ-ray flux the contributions of electron bremsstrahlung and inverse Compton which are much more uncertain than the hadronic contribution. The spread in their predictions reaches one order of magnitude at sub-Gev energies. We plan to investigate that problem in a future publication. We scrutinized here the various sources of error on the predictions of the hadronic component that dominates at GeV-TeV energies and stressed the importance of CR measurements and studies of the astrophysical sources of the Galactic plane, like supernova remnants.

References

Abdo, A. A., Ackermann, M., Ajello, M., et al. 2009, Physical Review Letters, 103, 251101
Abdo, A. A., Ackermann, M., Ajello, M., et al. 2010, ApJ, 710, 133
Abdo, A. A. et al. 2009, Astrophys. J., 703, 1249
Ahn, H. S. et al. 2010, Astrophys. J., 714, L89
Badhwar, G. D., Golden, R. L., & Stephens, S. A. 1977, Phys. Rev. D, 15, 820
Bertsch, D. L., Dame, T. M., Fichtel, C. E., et al. 1993, ApJ, 416, 587
Bissantz, N., Englmaier, P., & Gerhard, O. 2003, MNRAS, 340, 949
Blattnig, S. R., Swaminathan, S. R., Kruger, A. T., Ngom, M., & Norbury, J. W. 2000, Phys. Rev., D62, 094030
Boselli, A., Lequeux, J., & Gavazzi, G. 2002, A&A, 384, 33
Brogan, C. L., Gelfand, J. D., Gaensler, B. M., Kassim, N. E., & Lazio, T. J. W. 2006, ApJ, 639, L25
Case, G. L. & Bhattacharya, D. 1998, ApJ, 504, 761
Casse, F., Lemoine, M., & Pelletier, G. 2002, Phys. Rev., D65, 023002
Castellina, A. & Donato, F. 2005, Astropart. Phys., 24, 146
Cordes, J. M. & Lazio, T. J. W. 2002, ArXiv Astrophysics e-prints astro-ph/0207156
Cumberbatch, D. T., Tsai, Y.-L. S., & Roszkowski, L. 2010, Phys. Rev., D82, 103521
Dame, T. M., Hartmann, D., & Thaddeus, P. 2001, ApJ, 547, 792
Delahaye, T., Lavalle, J., Lineros, R., Donato, F., & Fornengo, N. 2010, A&A, 524, A51+
Delahaye, T. et al. 2009, Astron. Astrophys., 501, 821
Dickey, J. M., McClure-Griffiths, N. M., Gaensler, B. M., & Green, A. J. 2003, ApJ, 585, 801
Donato, F., Fornengo, N., Maurin, D., Salati, P., & Taillet, R. 2004, Phys. Rev. D, 69, 063501
Donato, F., Maurin, D., Brun, P., Delahaye, T., & Salati, P. 2009, Phys. Rev. Lett., 102, 071301
Donato, F. & Serpico, P. D. 2011, Phys. Rev. D, 83, 023014
Donato, F. et al. 2001, Astrophys. J., 563, 172
Feinstein, F., Fiasson, A., Gallant, Y., et al. 2009, in American Institute of Physics Conference Series, Vol. 1112, American Institute of Physics Conference Series, ed. D. Bastieri & R. Rando, 54–62
Gaisser, T. K. & Schaefer, R. K. 1992, ApJ, 394, 174
Gibson, S. J., Taylor, A. R., Higgs, L. A., & Dewdney, P. E. 2000, ApJ, 540, 851
Glover, S. C. O. & Mac Low, M. 2010, ArXiv e-prints 1003.1340
Green, D. A. 2009, Bulletin of the Astronomical Society of India, 37, 45
Grenier, I. A., Casandjian, J., & Terrier, R. 2005, Science, 307, 1292
Honda, M., Kajita, T., Kasahara, K., & Midorikawa, S. 2004, Phys. Rev., D70, 043008
Huang, C.-Y., Park, S. E., Pohl, M., & Daniels, C. D. 2007, Astropart. Phys., 27, 429
Hunter, S. D., Bertsch, D. L., Catelli, J. R., et al. 1997, ApJ, 481, 205
Incagli, M. 2010, AIP Conf. Proc., 1223, 43
Israel, F. P. 1997, A&A, 328, 471
Kalberla, P. M. W., Burton, W. B., Hartmann, D., et al. 2005, A&A, 440, 775
Kalberla, P. M. W. & Kerp, J. 2009, ARA&A, 47, 27
Kamae, T., Karlsson, N., Tsunefumi, M., Toshinori, A., & Tatsumi, K. 2006, ApJ, 647, 692
Knödlseder, J. & for the Fermi/LAT Collaboration. 2010, ArXiv e-prints: 1006.2635
Lavalle, J. 2010, ArXiv e-prints:1011.3063
Lorimer, D. R. 2004, in IAU Symposium, Vol. 218, Young Neutron Stars and Their Environments, ed. F. Camilo & B. M. Gaensler, 105–+
Manchester, R. N., Hobbs, G. B., Teoh, A., & Hobbs, M. 2005, AJ, 129, 1993
Maurin, D., Donato, F., Taillet, R., & Salati, P. 2001, Astrophys. J., 555, 585
Maurin, D., Taillet, R., Donato, F., et al. 2002, ArXiv Astrophysics e-prints: astro-ph/0212111
Mori, M. 2009, Astropart. Phys., 31, 341
Moskalenko, I. V. & Strong, A. W. 1998, ApJ, 493, 694
Moskalenko, I. V., Strong, A. W., Ormes, J. F., & Potgieter, M. S. 2002, ApJ, 565, 280
Nakamura, K. et al. 2010, J. Phys., G37, 075021

Nakanishi, H. & Sofue, Y. 2006, PASJ, 58, 847
Norbury, J. W. & Townsend, L. W. 2007, Nucl. Instrum. Meth., B254, 187
Orth, C. D. & Buffington, A. 1976, ApJ, 206, 312
Paczynski, B. 1990, ApJ, 348, 485
Panov, A. D. et al. 2009, Bulletin of the Russian Academy of Science, Phys., 73, 564
Perelstein, M. & Shakya, B. 2010, Phys. Rev. D, 82, 043505
Planck Collaboration, Ade, P. A. R., Aghanim, N., et al. 2011, ArXiv e-prints: 1101.2029
Pohl, M., Englmaier, P., & Bissantz, N. 2008, ApJ, 677, 283
Putze, A., Derome, L., & Maurin, D. 2010, A&A, 516, A66+
Roesler, S., Engel, R., & Ranft, J. 2001, prepared for 27th International Cosmic Ray Conference (ICRC 2001), Hamburg, Germany, 7-15 Aug 2001
Roesler, S., Engel, R., & Ranft, J. 2001, in Advanced Monte Carlo for Radiation Physics, Particle Transport Simulation and Applications., ed. A. Kling, F. Barão,
    M. Nakagawa, L. Távora, & P. Vaz, 1033–+
Sasaki, M. & Breitschwerdt, D. 2003, in International Cosmic Ray Conference, Vol. 5, International Cosmic Ray Conference, 2639–+
Shetty, R., Glover, S. C., Dullemond, C. P., & Klessen, R. S. 2010, ArXiv e-prints: 1011.2019
Shikaze, Y. et al. 2007, Astropart. Phys., 28, 154
Sodroski, T. J., Odegard, N., Arendt, R. G., et al. 1997, ApJ, 480, 173
Sodroski, T. J., Odegard, N., Dwek, E., et al. 1995, ApJ, 452, 262
Stecker, F. W. 1970, Astrophys. Space Sci., 6, 377
Stecker, F. W. 1973, ApJ, 185, 499
Stecker, F. W. 1977, ApJ, 212, 60
Stecker, F. W. & Jones, F. C. 1977, ApJ, 217, 843
Strong, A. W. 2011, ArXiv e-prints: 1101.1381
Strong, A. W., Bloemen, J. B. G. M., Dame, T. M., et al. 1988, A&A, 207, 1
Strong, A. W. & Moskalenko, I. V. 1998, ApJ, 509, 212
Strong, A. W., Moskalenko, I. V., Reimer, O., Digel, S., & Diehl, R. 2004, A&A, 422, L47
Strong, A. W., Porter, T. A., Digel, S. W., et al. 2010, ApJ, 722, L58
Tibaldo, L., Grenier, I. A., & for the Fermi LAT Collaboration. 2009, ArXiv e-prints: 0907.0312
Tibaldo, L., Grenier, I. A., Mizuno, T., & for the Fermi LAT collaboration. 2010, ArXiv e-prints: 1012.0455
Trotta, R., Jóhannesson, G., Moskalenko, I. V., et al. 2011, ApJ, 729, 106
Yusifov, I. & Küçük, I. 2004, A&A, 422, 545